remote sensing

MDPI

Article

Aerosols in the Mixed Layer and Mid-Troposphere from Long-Term Data of the Italian Automated Lidar-Ceilometer Network (ALICENET) and Comparison with the ERA5 and CAMS Models

Annachiara Bellini [1,2,3], Henri Diémoz [3], Gian Paolo Gobbi [2], Luca Di Liberto [2], Alessandro Bracci [2] and Francesca Barnaba [2,*]

[1] Department of Information Engineering, Electronics and Telecommunications, University 'La Sapienza', 00184 Rome, Italy; a.bellini@arpa.vda.it
[2] National Research Council-Institute of Atmospheric Science and Climate (CNR-ISAC), 00133 Rome, Italy; luca.diliberto@cnr.it (L.D.L.); alessandro.bracci@cnr.it (A.B.)
[3] ARPA Valle d'Aosta, 11020 Saint-Christophe, Italy; h.diemoz@arpa.vda.it
* Correspondence: francesca.barnaba@cnr.it

Abstract: Aerosol vertical stratification significantly influences the Earth's radiative balance and particulate-matter-related air quality. Continuous vertically resolved observations remain scarce compared to surface-level and column-integrated measurements. This work presents and makes available a novel, long-term (2016–2022) aerosol dataset derived from continuous (24/7) vertical profile observations from three selected stations (Aosta, Rome, Messina) of the Italian Automated Lidar-Ceilometer (ALC) Network (ALICENET). Using original retrieval methodologies, we derive over 600,000 quality-assured profiles of aerosol properties at the 15 min temporal and 15 metre vertical resolutions. These properties include the particulate matter mass concentration (PM), aerosol extinction and optical depth (AOD), i.e., air quality legislated quantities or essential climate variables. Through original ALICENET algorithms, we also derive long-term aerosol vertical layering data, including the mixed aerosol layer (MAL) and elevated aerosol layers (EALs) heights. Based on this new dataset, we obtain an unprecedented, fine spatiotemporal characterisation of the aerosol vertical distributions in Italy across different geographical settings (Alpine, urban, and coastal) and temporal scales (from sub-hourly to seasonal). Our analysis reveals distinct aerosol daily and annual cycles within the mixed layer and above, reflecting the interplay between site-specific environmental conditions and atmospheric circulations in the Mediterranean region. In the lower troposphere, mixing processes efficiently dilute particles in the major urban area of Rome, while mesoscale circulations act either as removal mechanisms (reducing the PM by up to 35% in Rome) or transport pathways (increasing the loads by up to 50% in Aosta). The MAL exhibits pronounced diurnal variability, reaching maximum (summer) heights of >2 km in Rome, while remaining below 1.4 km and 1 km in the Alpine and coastal sites, respectively. The vertical build-up of the AOD shows marked latitudinal and seasonal variability, with 80% (30%) of the total AOD residing in the first 500 m in Aosta-winter (Messina-summer). The seasonal frequency of the EALs reached 40% of the time (Messina-summer), mainly in the 1.5–4.0 km altitude range. An average (wet) PM > 40 μg m^{-3} is associated with the EALs over Rome and Messina. Notably, 10–40% of the EAL-affected days were also associated with increased PM within the MAL, suggesting the entrainment of the EALs in the mixing layer and thus their impact on the surface air quality. We also integrated ALC observations with relevant, state-of-the-art model reanalysis datasets (ERA5 and CAMS) to support our understanding of the aerosol patterns, related sources, and transport dynamics. This further allowed

check for updates

Academic Editors: Min Xie, Jane Liu and Bingliang Zhuang

Received: 13 December 2024
Revised: 13 January 2025
Accepted: 18 January 2025
Published: 22 January 2025

Citation: Bellini, A.; Diémoz, H.; Gobbi, G.P.; Di Liberto, L.; Bracci, A.; Barnaba, F. Aerosols in the Mixed Layer and Mid-Troposphere from Long-Term Data of the Italian Automated Lidar-Ceilometer Network (ALICENET) and Comparison with the ERA5 and CAMS Models. *Remote Sens.* **2025**, *17*, 372. https://doi.org/10.3390/rs17030372

Copyright: © 2025 by the authors. Licensee MDPI, Basel, Switzerland. This article is an open access article distributed under the terms and conditions of the Creative Commons Attribution (CC BY) license (https://creativecommons.org/licenses/by/4.0/).

measurement vs. model intercomparisons and relevant examination of discrepancies. A good agreement (within 10–35%) was found between the ALICENET MAL and the ERA5 boundary layer height. The CAMS PM_{10} values at the surface level well matched relevant in situ observations, while a statistically significant negative bias of 5–15 μg m^{-3} in the first 2–3 km altitude was found with respect to the ALC PM profiles across all the sites and seasons.

Keywords: aerosol vertical layering; ALICENET; Mediterranean; air quality; CAMS; ERA5

1. Introduction

Atmospheric aerosols are a key component of the Earth's climate system, influencing the planetary radiative budget [1] and the hydrological cycle [2,3]. They also substantially impact air quality and human health [4,5]. These climate and air quality effects depend directly or indirectly on the aerosols' optical and physical properties, exhibiting significant spatiotemporal variability. For these reasons, aerosol extinction and its vertical integral, the aerosol optical depth (AOD), are recognised as essential climate variables (ECVs; [6]) requiring continuous, long-term monitoring [7]. These parameters are fundamental for understanding aerosol–radiation interactions [8] and their subsequent effects on the climate [9]. Concurrently, the aerosol mass concentration, or PM, is a key metric for assessing air quality and related human health impacts, leading to strict monitoring standards and regulatory limits worldwide [10,11].

The vertical distribution of aerosols is particularly significant from both the climatic and air quality perspectives. From a climate point of view, aerosol stratification fundamentally influences radiative transfer processes [12] and aerosol–cloud interactions [3,13,14]. High-altitude ecosystems are also affected through deposition processes [15,16]. Elevated aerosol layers can significantly alter the atmospheric thermal structure and stability, with substantial implications for local and regional climates [17,18]. From an air quality perspective, understanding the vertical distribution of aerosols is essential for analysing the influence of medium- to large-scale transport dynamics [19–21], dilution processes within the mixing layer [22], and aerosol formation and growth mechanisms aloft [23,24] on the surface PM concentrations. Given the more stringent air quality PM standards in the recently approved EU Directive 2024/2881/EC [11], the capability to detect and quantify contributions from non-local sources becomes increasingly important for effective air quality management. Vertical profile information may support the identification of locally produced and transported pollution [25,26], including transboundary advections of natural particles, facilitating more targeted and efficient mitigation strategies.

Furthermore, accurate observation-based characterisation of the aerosol vertical structure is crucial for improving satellite-based retrievals of air-quality-relevant quantities [27–30] and atmospheric model parameterisations and assimilation abilities [31], ultimately leading to more reliable aerosol datasets.

Despite its recognised importance, continuous and quantitative monitoring of aerosol vertical stratification remains scarce, particularly in some countries. Lidar networks such as ACTRIS-EARLINET in the EU provide high-quality measurements [32] on a regular basis, but their spatial and temporal coverage is still insufficient to capture the full four-dimensional variability of aerosols and related atmospheric processes. This is particularly important for air quality assessments requiring continuous, high-temporal resolution PM monitoring through dense networks. Furthermore, long-term profile observations within vast networks could provide insights into emission trends and the effectiveness of air quality

policies, as demonstrated by initiatives such as the Integrated Carbon Observation System (ICOS; [33]). Currently, aerosol profile observations are not included in standard air quality monitoring protocols. This observational gap may hinder understanding of aerosol-related atmospheric processes and the effectiveness of air quality forecasting and management strategies. Some efforts to demonstrate the added value of profiling measurements in support of air quality are currently being performed in the framework of the ongoing EC H2020 RIURBANS project (2021–2025, https://riurbans.eu/ (accessed on 13 January 2025)), which aims at developing an air quality monitoring system that complements those currently available.

Automated lidar ceilometers (ALCs) offer a promising solution to complement networks of research-oriented lidars and standard in situ air quality systems, providing continuous aerosol profiles with increasing quantitative retrieval capabilities [34]. Currently, large-scale ALC networks, such as the European EUMETNET E-PROFILE (https://e-profile.eu/ (accessed on 13 January 2025)), enable operational aerosol monitoring at a continental scale with high temporal resolution. These systems effectively capture the mixing layer dynamics [22], provide comprehensive datasets for tracking aerosol-related phenomena [35], and support improvements in atmospheric and chemistry models [36,37].

The potential of ALC networks to advance atmospheric science and air quality management is indeed increasingly recognised across the scientific community. For instance, the EC Horizon 2020 CAMAERA project specifically envisions enhancing vertical aerosol representation in models through ALC data assimilation [38]. Furthermore, the high-resolution, continuous monitoring of boundary layer dynamics provided by ALC systems has proved valuable across multiple domains, including air quality assessment and renewable energy production [39,40]. This expanding recognition underscores the value of continuous, vertically resolved aerosol observations for scientific research and practical applications in different societal fields (i.e., human health, solar energy production).

In Italy, the Automated Lidar-Ceilometer Network (ALICENET, https://www.alice-net.eu/ (accessed on 13 January 2025)) was established in 2015 by the National Research Council-Institute of Atmospheric Sciences and Climate (CNR-ISAC) to provide continuous monitoring of aerosol vertical profiles across the country using state-of-the-art ALC systems. ALICENET operates as a collaborative, open consortium with active contributions from diverse atmospheric science and monitoring institutions, including regional environmental protection agencies (EPAs), universities, and research centres.

ALICENET's strategically distributed monitoring sites enable comprehensive investigation of aerosol vertical distributions across diverse Italian environments. In the current configuration, the network covers small-to-large urban areas from northern to southern Italy, including the main cities within the heavily polluted Po Basin and its surroundings (Turin, Milan, Genoa), providing detailed insights into the PM dynamics in densely populated regions [20,21]. The ALICENET stations in central and southern Italy are well positioned to monitor the vertical structure of long-range transported desert dust from North Africa [19,41]. Coastal sites allow for the investigation of the vertical mixing of marine aerosols with continental air masses, while multiple sites near Mount Etna in Sicily allow for the detection of volcanic ash layers [42].

A key strength of ALICENET is its tailored and centralised data processing, which enables homogeneous and quantitative retrieval of aerosol optical and physical properties and vertical layering information through established methodologies described in detail in previous studies [43,44]. This approach ensures consistency in data quality across the network, facilitating robust comparative studies between different sites over the short and long term.

This work presents and makes available a new long-term (2016–2022) observational dataset of aerosol vertical profiles across Italy, based on continuous ALICENET measurements at high vertical (15 m) and temporal (15 min) resolution. The main objectives of the study are (1) to demonstrate the maturity of the ALC technique for quantitative aerosol monitoring over the long term; (2) to comprehensively characterise the aerosol vertical distributions and variability across Italy through long-term ALC observations; and (3) to integrate and intercompare these long-term observations with reference model reanalysis data to better understand the aerosol sources and transport dynamics and evaluate observations–models consistencies.

To achieve these objectives, we selected high-quality ALC data from three ALICENET stations spanning from north to south Italy (Section 2.1). We homogeneously processed their multiannual (2016–2022) instrumental records using ALICENET retrieval methodologies (Section 2.2), and complemented them with relevant, long-term atmospheric and chemistry model reanalysis data (Section 2.3). Specifically, we employed the fifth-generation atmospheric reanalysis (ERA5), produced by the European Centre for Medium-Range Weather Forecasts (ECMWF), and the European air quality reanalysis produced by the Copernicus Atmosphere Monitoring Service (CAMS), two reference datasets for climate and air quality studies [45,46]. Through comprehensive analysis of these long-term observational and model datasets, we derived the key characteristics and driving mechanisms of aerosol stratifications (Section 3). Specifically, we characterised the aerosol mass concentrations (Section 3.1), extinction profiles and column-integrated AOD (Section 3.2), and layering structures (Section 3.3), including the mixed and elevated aerosol layers. Finally, in Section 4, we summarise our results and draw conclusions.

The main novelties of this work stem from four main aspects: (a) extensive temporal coverage through continuous (24/7), 7-year, high-resolution profile observations; (b) quantitative retrieval of essential aerosol properties (mass and extinction profiles plus vertical layering) using original methodologies developed within ALICENET; (c) comprehensive characterisation of aerosol vertical distributions from the sub-hourly to seasonal timescales across diverse environments (Alpine, urban, and coastal); and (d) combined use of the new (shared) observational dataset and state-of-the-art model reanalysis products to extend the aerosol characterisation and explore the measurement–model consistency along the vertical dimension.

2. Materials and Methods

In this section, we (a) describe the ALICENET observations and ancillary measurements used to characterise the aerosol field at the study sites (Section 2.1); (b) provide an overview of the methodologies for retrieving aerosol properties and layering, along with additional quality assurance procedures applied to refine the dataset for long-term statistical analysis (Section 2.2); and (c) introduce the model-based datasets used to complement the observational analysis (Section 2.3).

2.1. Sites and Instruments

The ALICENET stations are strategically distributed across Italy from north to south (Figure 1), enabling the monitoring of aerosol vertical distributions under diverse atmospheric conditions within the Central Mediterranean region [43]. For this work, we selected three stations (Aosta, Rome, and Messina; Table 1) located in the northern, central and southern parts of the peninsula. These stations were chosen from among those with the most continuous, high-quality ALC records.

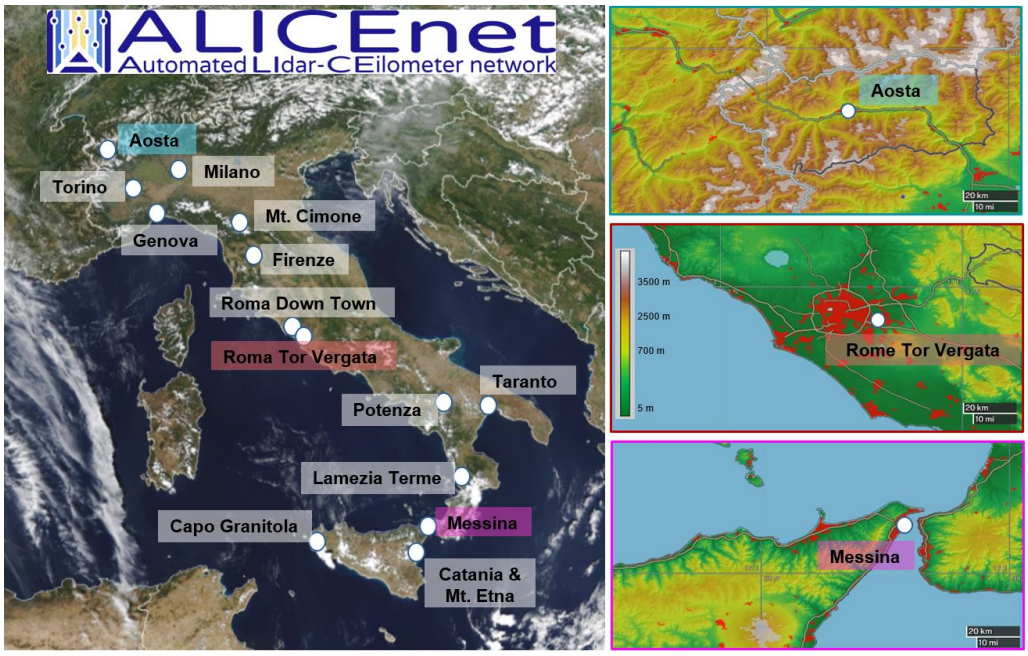


Figure 1. Location and naming of the ALICENET stations (**left**) and composite zooms over the three selected stations (**right**) showing the topography (inset legend) and urbanised areas (reddish shaded areas). Background map credits: (**left**) NASA/NOAA Suomi-NPP VIIRS; and (**right**) NASA Worldview combining the Global Digital Elevation Model colour index and colour-shaded relief (inset legend) from the ASTER and urban land cover (red overlaid areas) from the Terra and Aqua combined MODIS Land Cover Type.

Table 1. ALICENET station characteristics and ancillary measurements used for the analysis.

ALICENET Station (Reference Institution)	Site Type (Inhabitants)	Lat, Lon	Altitude a.s.l.	ALC Instrument (Operating Period)	Ancillary, Additional Instrumentation Used Here (Reference Network and Distance from ALC)
Aosta (ARPA Valle d'Aosta)	semi-rural, Alpine, Aosta outskirts (40 k)	45°44′N, 07°21′E	560 m	CHM15k (2015–present)	- solar photometer (SKYNET, co-located) - PM10 and meteorological measurements (Regional EPA site 'Aosta–Downtown', 5 km distance)
Rome Tor Vergata (CNR-ISAC)	urban background, Rome outskirts (2.9 M)	41°50′N, 12°38′E	100 m	CHM15k (2013–present)	- solar–lunar photometer (AERONET, co-located) - meteorological measurements (Regional EPA, co-located) - PM10 (Regional EPA site 'Cinecittà', 8 km distance)
Messina (CNR-ISAC, CNR-IRBIM)	urban, maritime, near Messina harbour (230 k)	38°11′N, 15°34′E	5 m	CHM15k (2016–present)	- solar photometer (AERONET, 10 km distance) - PM10 and meteorological measurements (Regional EPA site 'Villa Dante', 6 km distance)

The northernmost station, Aosta, is operated by the Regional Environmental Protection Agency of the Aosta Valley (ARPA Valle d'Aosta) at a semi-rural site in the northwestern Italian Alps. Situated in a broad east–west-oriented Alpine valley surrounded by mountains reaching over 4000 m, this location experiences distinctive atmospheric circulation patterns characterised by frequent mountain–valley breezes and Föhn events. While generally experiencing clean air conditions, the site can be affected by local pollution sources, such

as traffic and residential heating, and by regional transport of aerosols from the heavily industrialised Po Valley to the southeast [20,21]. The complex terrain and atmospheric dynamics make this station particularly interesting for studying atmosphere–orography interactions and the impact of transported pollution on pristine mountain environments.

The Rome Tor Vergata Station (hereafter Rome) is situated at the CNR-ISAC Atmospheric Observatory, approximately 10 km southeast of Rome's city centre, in one of Italy's most urbanised regions. Located at the edge of a hilly area south of Rome and roughly 25 km inland from the Tyrrhenian Sea, the station experiences daily breeze regimes. Its Mediterranean climate is characterised by hot, dry summers and mild, humid winters. The site is mainly influenced by anthropogenic (traffic, domestic heating) and natural (desert dust) aerosol sources [19,41,47]. Its position enables the study of urban aerosol dynamics, the interactions between urban and rural air masses, and the influence of long-range transported particles. The proximity to the sea also provides opportunities to investigate the impact of marine aerosols and sea breeze circulations on urban air quality [48].

The Messina Station is located on the northeastern coast of Sicily, at the confluence of the Ionian and Tyrrhenian Seas. This urban, harbour, coastal site sits within a complex geographical setting, bordered by the Strait of Messina to the east and the Peloritani Mountains to the west. The local climate is typically Mediterranean. The site is affected by diverse aerosol sources, including maritime aerosols, urban pollution, and frequent intrusions of Saharan dust. Its proximity to the active Mount Etna (about 75 km to the south) and Stromboli Volcano (110 km to the north) also allows for the occasional observation of volcanic aerosols. The distinctive position of Messina in the narrow strait creates unique wind patterns and atmospheric circulations that significantly influence the transport and mixing of aerosols in the area.

At all the selected stations, continuous aerosol profile observations were conducted using CHM15k ALC systems (manufactured by OTT Hydromet GmbH, Kempten, Germany). These single-channel, bistatic instruments probe the atmosphere with high temporal and vertical resolution (15 s and 15 m, respectively) and provide good data quality from 0.2 km (where the laser beam begins to fully overlap with the telescope field of view) up to 7–8 km above ground level. The complementary instrumentation used in this study included photometers operating within the international networks AERONET [49] and SKYNET [50], as well as in situ PM samplers operated by regional environmental protection agencies (EPAs). Table 1 details the selected ALICENET sites and instruments, including information about the ancillary instrumentation used in this study, co-located with or near the ALC systems.

2.2. ALICENET Data Processing and Long-Term Statistics

ALICENET implements a specifically developed, centralised data processing chain to derive quantitative information on aerosol properties and vertical layering from ALC observations. As extensively described in [43], this process includes several key steps: pre-processing, absolute calibration, retrieval of aerosol properties, and automatic detection of aerosol layers. The main output products range from aerosol optical and physical properties to aerosol layering information.

The pre-processing procedures encompass cloud screening, signal denoising and overlap correction in the lowermost levels. The first two procedures filter out data with a low signal-to-noise ratio (SNR) and, if necessary, vertical ranges from 500 m below the cloud base height upwards. The third procedure corrects for incomplete superposition of the laser beam and telescope field of view in bistatic ALCs such as the CHM15k used here. This correction is implemented through an instrument-specific, temperature-dependent overlap correction function [51].

The absolute calibration employs a Rayleigh methodology, comparing the pre-processed ALC signals with theoretical molecular profiles in aerosol-free regions between 3 and 7 km in altitude. An iterative algorithm automatically selects suitable molecular windows, and specific quality controls ensure the absence of aerosol layers therein. The calibration coefficient is then derived using backward Klett inversion [52] within the selected molecular window.

The aerosol optical properties are retrieved through forward inversion [34] of the calibrated signals, solving the elastic lidar equation using ALICENET-specific functional relationships linking extinction and backscatter [44]. This approach retrieves the aerosol backscatter, extinction and optical depth without requiring ancillary data or a priori assumptions on the extinction-to-backscatter ratio. Similar functional relationships link the aerosol backscatter to relevant physical properties (surface area, volume, and thus mass, concentrations). Since ALCs sound aerosol particles in real atmospheric conditions, hygroscopic correction is necessary when comparing ALC-retrieved aerosol mass to (dry) in situ PM measurements. In ALICENET, this is performed as follows [53]:

$$\mathrm{PM}^{\mathrm{dry}} = \frac{\mathrm{PM}}{1 + \frac{1}{\rho}\left(\mathrm{GF}^3 - 1\right)} \tag{1}$$

where

$$\mathrm{GF} = \left(1 - \frac{\mathrm{RH}}{100}\right)^{-\gamma} \tag{2}$$

is the hygroscopic growth factor, PM is the ALC-based mass estimate, RH is the ambient relative humidity, ρ is the aerosol density, and γ is the hygroscopic exponent [53].

The aerosol vertical layering is determined through an ALICENET original automatic aerosol layer detection (ALADIN) algorithm. This algorithm, using aerosols as tracers, identifies three main layer types:

1. The mixed aerosol layer (MAL), a layer where aerosols are well mixed by turbulent fluxes.
2. The elevated aerosol layers (EALs), structures of enhanced aerosol concentrations located above the MAL.
3. The continuous aerosol layer (CAL), the maximum altitude affected by aerosols, above which the atmosphere is thus aerosol-free.

Operatively, the CAL is identified as the region where the total backscatter exceeds the molecular backscatter for at least 98% of its extension. The MAL is identified using dynamic time warping [54] and variance analyses of the backscatter profiles over 30 min windows. The EALs are detected through continuous wavelet transform [55] to identify the signal peaks attributable to the aerosol layers, followed by an iterative technique determining the layer boundaries based on the backscatter profiles.

Four main factors affect ALC data quality. First, the incomplete overlap between the laser beam and the telescope field of view impacts signal quality in the first 600–800 m. However, instrument-specific corrections effectively mitigate this limitation, as confirmed by comparison with surface measurements. Second, signal noise generally affects measurements above 6–7 km altitude. Thus, we focus here on the 0–5 km range where the signal-to-noise ratio is robust. Also, note that the relative impact of signal noise is higher with lower aerosol concentrations but significantly reduced for strong signals like in the presence of EALs. Third, accurate signal calibration is essential for correct aerosol retrievals. The uncertainty of the ALICENET calibration procedure aligns with international standards. Fourth, since the current retrieval of aerosol properties is optimised for continental-type aerosols, it may underestimate the contributions of irregular particles (e.g., dust) to ex-

tinction and mass. For the PM, additional uncertainty arises from assumptions about the aerosol density. While this affects the absolute values along the profile, the signal shape remains reliable, thus not impacting the layer detection capabilities. The overall data quality is confirmed by the good agreement between ALICENET products and independent measurements, including surface PM data and AERONET/SKYNET AOD observations, as reported in previous studies [43,44] and in the following Section 3. Overall, the estimated uncertainties for the ALICENET products range from 20% for attenuated backscatter to 30–40% for optical properties and up to 50% for mass concentrations.

In this work, we homogeneously processed the multiannual ALICENET measurements of the selected stations to derive the associated aerosol quantities. Specifically, we retrieved vertical profiles of the aerosol extinction and volume concentrations at 15 min temporal and 15 m vertical resolution, requiring SNR > 20%. The PM concentrations were derived from the estimated aerosol volume using a particle density $\rho = 1.5$ g cm^{-3}. A hygroscopic correction (Equations (1) and (2)) was applied using a growth factor $\gamma = 0.2$ [56] and relative humidity profiles from models (ERA5 reanalysis for Rome and Messina, and MERIDA reanalysis for Aosta, see Section 2.3).

The identification of the MAL, CAL, and EALs was performed at 15, 30, and 60 min resolutions, respectively. Since identifying EALs uses a reference backscatter profile [43], the current analysis employs site- and season-dependent median backscatter profiles derived from the full 7-year records.

Examples of the ALICENET products derived as detailed above are given in Figure 2, referring to data collected at the Rome Tor Vergata site between 14 and 21 October 2022. It shows the vertical profiles (0–5 km, y-axis) of (a) the aerosol extinction coefficient at 1064 nm, (b) the PM concentrations, (c) the column-integrated extinction (i.e., AOD, which is also compared to the reference Level 2 AOD from the co-located AERONET sunphotometer), and (d) the ALADIN atmospheric scene classification, including the MAL, CAL, EALs, as well as aerosol-free (molecular, MOL) and cloud-filtered (CLOUD) regions.

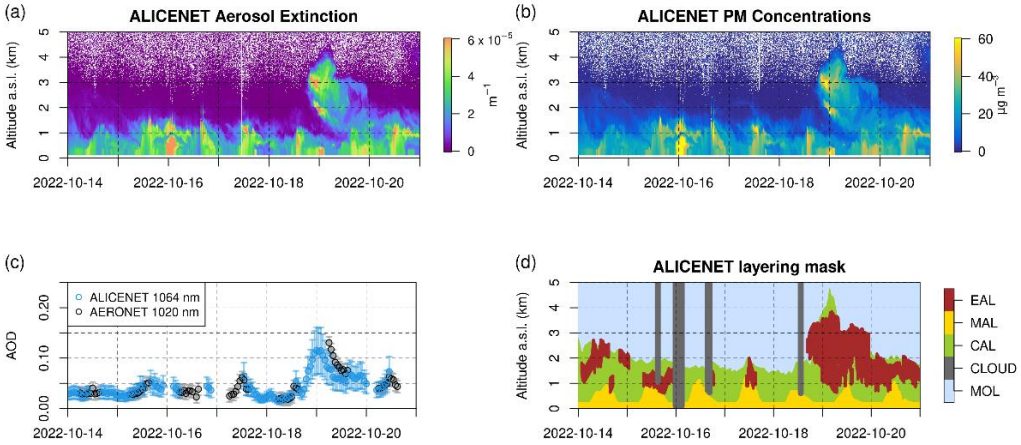


Figure 2. ALICENET aerosol products derived from measurements performed in Rome Tor Vergata, 14–21 October 2022: (**a**) aerosol extinction profiles at 1064 nm, (**b**) PM profiles, (**c**) hourly averaged ALICENET-derived AOD (blue) and AERONET L2 AOD (black) from the co-located sunphotometer, and associated uncertainties (error bars), and (**d**) aerosol layering mask derived by the ALICENET-ALADIN tool, discriminating the continuous aerosol layer (CAL), mixed aerosol layer (MAL), elevated aerosol layers (EALs), aerosol-free (i.e., molecular, MOL) and cloud-screened (CLOUD) regions.

The ALICENET data in Figure 2 show shallow aerosol layers in the lower troposphere and MAL heights below 1.5 km, consistent with fall conditions. On 18 October, an EAL associated with mass concentrations up to 60 μg m^{-3} appeared between 2 and 4 km a.s.l. It then descended and entered the MAL on 19 and 20 October.

To further ensure both the physical and statistical significance of the aerosol profiles and layer data throughout the 2016–2022 period, we established several quality assurance (QA) criteria (as reported in Appendix A.1). Table 2 summarises the resulting number of quality-assured data for the aerosol profiles and layering information (CAL, MAL, EALs) over the 7 years. The analysis incorporated over 200,000 quality-assured aerosol profiles (i.e., >80% data coverage) per site, with a sufficiently balanced distribution across seasons, months and hours of the day. The remaining 20% of data gaps stem from denoising and cloud screening procedures and the application of QA criteria. Appendix A.2 (Figure A1) provides a detailed picture of the cloud-screened data percentages for each site.

Table 2. Number of quality-assured aerosol profiles and layers (continuous aerosol layer, CAL, mixed aerosol layer, MAL, elevated aerosol layers, EALs) at each station over the period 2016–2022 and relevant, percentage distribution among the seasons.

ALICENET Station	Aerosol Profiles (15 min Resolution)	CAL (15 min Resolution)	MAL (30 min Resolution)	EAL (1 h Resolution)
Aosta	225,148 (23% winter, 25% spring, 27% summer, 25% fall)	181,826 (18% winter, 28% spring, 35% summer, 19% fall)	94,656 (24% winter, 24% spring, 27% summer, 25% fall)	8170 (9% winter, 29% spring, 37% summer, 25% fall)
Rome	222,415 (23% winter, 26% spring, 25% summer, 26% fall)	183,378 (22% winter, 26% spring, 28% summer, 24% fall)	94,279 (23% winter, 26% spring, 27% summer, 24% fall)	20,674 (10% winter, 28% spring, 39% summer, 23% fall)
Messina	200,706 (23% winter, 24% spring, 27% summer, 26% fall)	185,060 (22% winter, 24% spring, 30% summer, 24% fall)	39,684 (21% winter, 19% spring, 34% summer, 26% fall)	20,720 (8% winter, 22% spring, 45% summer, 25% fall)

For the long-term analysis, we employed standard statistical techniques, with particular emphasis on characterising the seasonal and diurnal variability along the vertical dimension. Our methodology involved calculating the mean, median, and interquartile values of the aerosol properties and layers from ground level to a 5 km altitude. This altitude aligns with the highest vertical level of CAMS data (see Section 2.3).

2.3. ERA5 and CAMS Model Reanalysis Datasets

As mentioned, we used model-based datasets to complement the observation-based analysis. In particular, for meteorological fields, we utilised the ECMWF-ERA5 reanalysis [57] produced as part of the C3S, Copernicus Climate Change Service [58]. ERA5 is widely used for climate studies and various applications, including air quality assessment and renewable energy planning. The reanalysis is based on the Integrated Forecasting System (IFS) and employs a 4D-Var data assimilation system that incorporates many observations from both in situ measurements and satellite data. ERA5 provides a comprehensive record of the global atmosphere from 1940 onwards at hourly intervals, with a horizontal resolution of $0.25^\circ \times 0.25^\circ$ and 137 vertical levels from the surface up to 0.01 hPa.

For atmospheric composition data, we employed the European air quality ensemble reanalysis produced by CAMS [59]. The dataset, available from 2018, is produced using an ensemble approach and assimilates surface in situ observations and satellite data. The ensemble methodology typically outperforms individual models by minimising model-specific biases [60], providing a robust representation of the air quality and atmospheric composition over Europe. Specifically, the CAMS European Ensemble dataset

is the median of 9 (11 from 2022) state-of-the-art regional air quality model outputs, namely CHIMERE [61], EMEP [62], EURAD-IM [63], LOTOS-EUROS [64], MATCH [65], MOCAGE [66], SILAM [67], DEHM [68], and GEM-AQ [69]. The CAMS reanalysis covers the European domain at $0.1^\circ \times 0.1^\circ$ resolution, providing hourly three-dimensional fields of key pollutants, including the PM_{10} and relevant dust and biomass-burning components. Note that the aerosol optical properties (e.g., AOD) are not included in the CAMS European Ensemble dataset.

As a first step, we evaluated the reliability of the ERA5 and CAMS model datasets in the study area through comparison with relevant available meteorological observations. For ERA5, the comparison of the wind fields with surface measurements revealed good agreement in Rome and Messina, where the terrain characteristics and the proximity to assimilated radiosonde measurements facilitated model accuracy. In the complex Alpine environment of Aosta, ERA5's coarse resolution proved insufficient to capture the observed breeze regime (see Figure A2 in Appendix A.2). Therefore, for Aosta, we opted to use the high-resolution atmospheric reanalysis MERIDA [70] produced by RSE ('Ricerca sul Sistema Energetico', [71]). This reanalysis is a dynamic downscaling produced through the Weather Research and Forecasting model. Its meteorological fields are available at pressure levels of 850, 700 and 500 hPa.

Table 3 provides details of the ERA5, MERIDA, and CAMS fields used in this work, including their vertical levels, spatial and temporal resolutions, and temporal coverage. The ERA5 and MERIDA models use pressure levels for vertical coordinates, while CAMS employs height levels above ground.

Table 3. Details of the model-based datasets used for the analysis.

Model Dataset	Vertical Levels	Horizontal Resolution	Temporal Resolution	Analysed Fields	Available Period
ERA5 atmospheric reanalysis	1000, 950, 900, 850, 800, 750, 700, 600, 500 hPa	$0.25^\circ \times 0.25^\circ$	Hourly	Geopotential, horizontal wind, relative humidity	2016–2022
MERIDA atmospheric reanalysis	850, 700, 500 hPa	$0.07^\circ \times 0.07^\circ$	Hourly	Geopotential, horizontal wind, relative humidity	2016–2022
CAMS European air quality Ensemble reanalysis	0, 250, 500, 1000, 2000, 3000, 5000 m a.g.l.	$0.1^\circ \times 0.1^\circ$	Hourly	PM_{10} and relevant vertically resolved components (dust, wildfire)	2018–2021 (validated) 2022 (interim)

As an example of the CAMS data, Figure 3 shows the modelled PM_{10} profiles and relevant dust component extracted for the Rome Tor Vergata site during the same period as presented in Figure 2. Figure 3 shows that CAMS effectively captures the presence and temporal evolution of the elevated layer observed by ALC between 18 and 21 October, further revealing its dust-dominated composition. However, the absolute values are lower compared to the ALC retrievals of the PM and, as expected, cannot reproduce the fine spatiotemporal scales of the observations, particularly in the first 2 km.

In general, CAMS reproduced the surface PM concentrations well (e.g., Section 3.1), benefiting from the assimilation of PM_{10} ground-based measurements within the ensemble models. Additional comparisons between the model datasets and the ALC-based products are given hereafter.

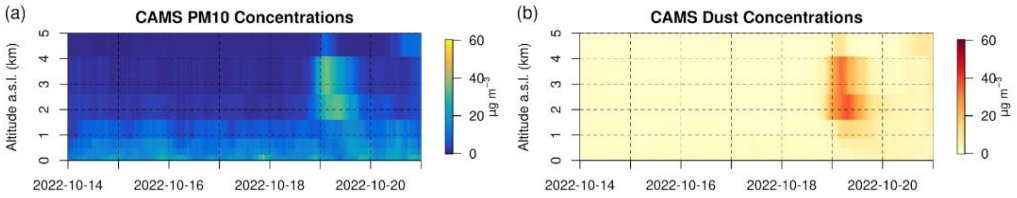


Figure 3. CAMS data of (**a**) the total PM_{10} and (**b**) the dust PM_{10} for the same site and period as presented in Figure 2.

3. Results

In this section, we present the results of our statistical analysis of the long-term (2016–2022), continuous, quality-assured ALICENET data on the aerosol mass concentrations (Section 3.1), optical properties (extinction/AOD, Section 3.2), and vertical layering (Section 3.3) across the three addressed geographical contexts. Our analysis primarily relies on high-resolution ALC observations, complemented by meteorological and atmospheric composition fields from the ERA5 and CAMS European air quality reanalyses.

3.1. Aerosol Mass Profiles from ALICENET Observations and Integration with Model Data

The monthly and daily resolved long-term analysis of the PM vertical profiles is summarised in Figure 4. This shows the ALC-based vertical profiles (0–5 km, y-axis) of the median (2016–2022) PM concentrations at the three selected sites, resolved by month (top x-axis) and time of day (bottom x-axis) at the 15 min temporal and 15 m vertical resolutions. The data reveal marked gradients in the absolute PM values across sites in both the lower and middle troposphere. At Aosta, the median PM values remain consistently below 15 µg m^{-3} throughout both the vertical profile and the annual cycle. In contrast, the southern sites exhibit substantially higher concentrations, exceeding 35 µg m^{-3} below 1 km during winter and maintaining levels above 20 µg m^{-3} at higher altitudes during summer. These patterns reflect the contrast between the relatively modest local emissions in Aosta and the more significant pollution sources at the southern sites, particularly in the urban environment of Rome, combined with the influence of large-scale aerosol transport across the Mediterranean region [72]. By illustrating the daily evolution of the PM vertical profiles, Figure 4 also reveals the effects of the turbulent mixing, mesoscale circulations and atmospheric stability conditions specific to each site.

At the Alpine site in Aosta (Figure 4a), weak turbulent fluxes are regularly overshadowed by mountain–valley breezes that develop during the afternoon. Previous studies showed that these breezes transport polluted air masses from the Po Valley and increase the PM concentrations during the latter half of the day [20,21]. This long-term perspective confirms this effect, which intensifies during summer months when the transported aerosol layers extend vertically up to 4 km a.s.l. In winter, shallow temperature inversions confine aerosols in the first 500 m.

The Rome site (Figure 4b) exhibits distinct modulation of the PM profiles driven by mixing processes and land–sea breezes from spring to autumn. During the warmest months, convection effectively dilutes the particle concentrations in the central part of the day, while sea breezes primarily act as an aerosol removal mechanism in the afternoon [48]. In winter, the observed afternoon/evening increase in aerosol mass mainly relates to enhanced biomass burning from agriculture and domestic heating [47], particle hygroscopic growth phenomena and a shallow mixing layer height.

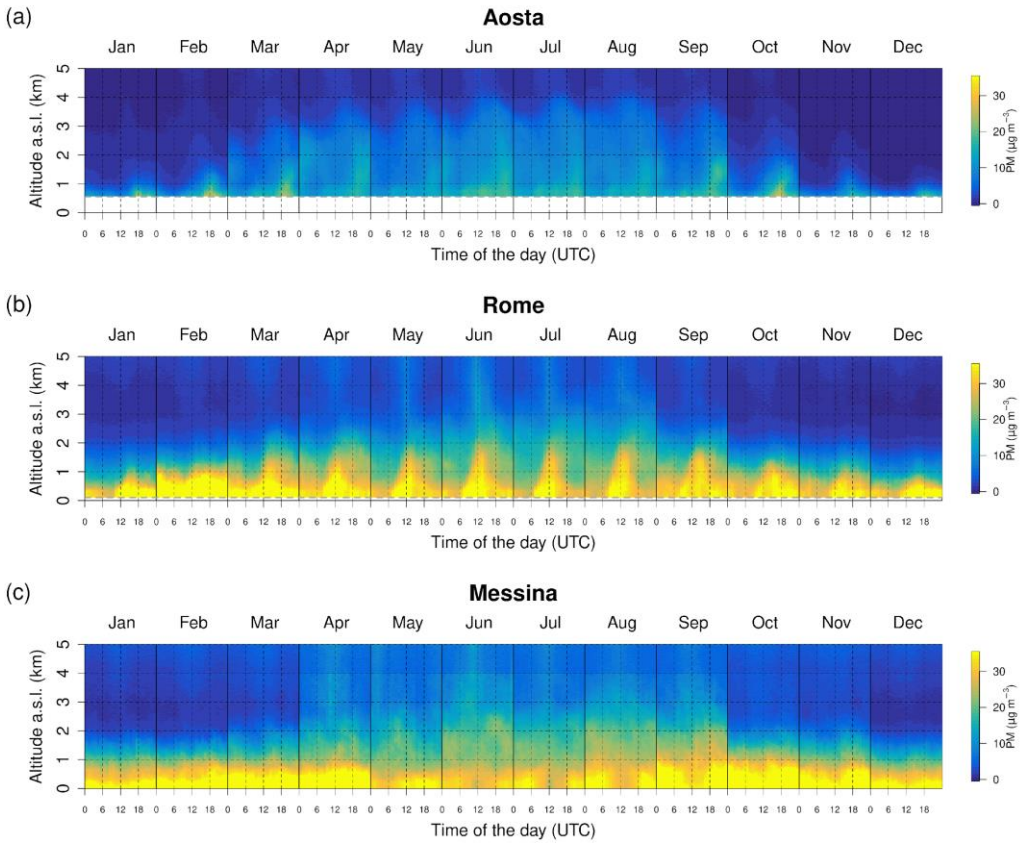


Figure 4. ALICENET-derived vertical profiles (0–5 km, y-axis) of the median (2016–2022) PM resolved by month (top x-axis) and time of day (bottom x-axis) in (**a**) Aosta, (**b**) Rome, and (**c**) Messina. The grey dashed lines indicate the ground level at each station.

As is typical of coastal locations, Messina (Figure 4c) displays a persistent marine layer that constrains mixing development over land [73], largely confining local aerosols to low levels (<1 km) throughout the year. During summer, daily modulation by land–sea breezes and hygroscopic effects is discernible within the first kilometre, while the increased aerosol loads throughout the atmospheric column relate to the frequent Saharan dust intrusions at this southern Mediterranean site ([41]; see also Section 3.3).

The development of these typical mesoscale dynamics at each site is confirmed by relevant, site-specific wind patterns derived from the model reanalyses and surface wind measurements, as shown in Figure 5. For Rome and Messina, we used ERA5 wind fields at six pressure levels between 1000 and 500 hPa, interpolated to fixed ALC vertical ranges. However, as anticipated, the complex Alpine orography makes ERA5 unsuitable for capturing the characteristic breeze regime at Aosta [74], requiring the use of higher-resolution wind fields from the MERIDA reanalysis at 850, 700, and 500 hPa (as detailed in Section 2.3). Surface-level measurements from the nearest meteorological station (Table 1) are shown in Figure 5 at the lowest vertical level in each panel.

Figure 5 shows the development of mountain–valley breezes in Aosta (from east to west during daytime, Figure 5a) and sea–land breezes in Rome (from west to east during daytime, Figure 5b) in the first 2 km. In Aosta, the mesoscale winds in the first 2 km decouple from the higher synoptic and opposing flows. In Rome, both sea–land breezes and synoptic flows predominantly blow from the west. A general increase in the wind intensity from north to south across the study sites is evident. In fact, the winds in the Po Valley are typically weak, as surrounding mountains obstruct synoptic circulations while promoting weaker thermally driven breezes. In Messina, the interaction between synoptic

flows and local orography (see Figure 1) generates intense, channelled flows through the Messina Strait, which superimpose on the daily breeze patterns (Figure 5c).

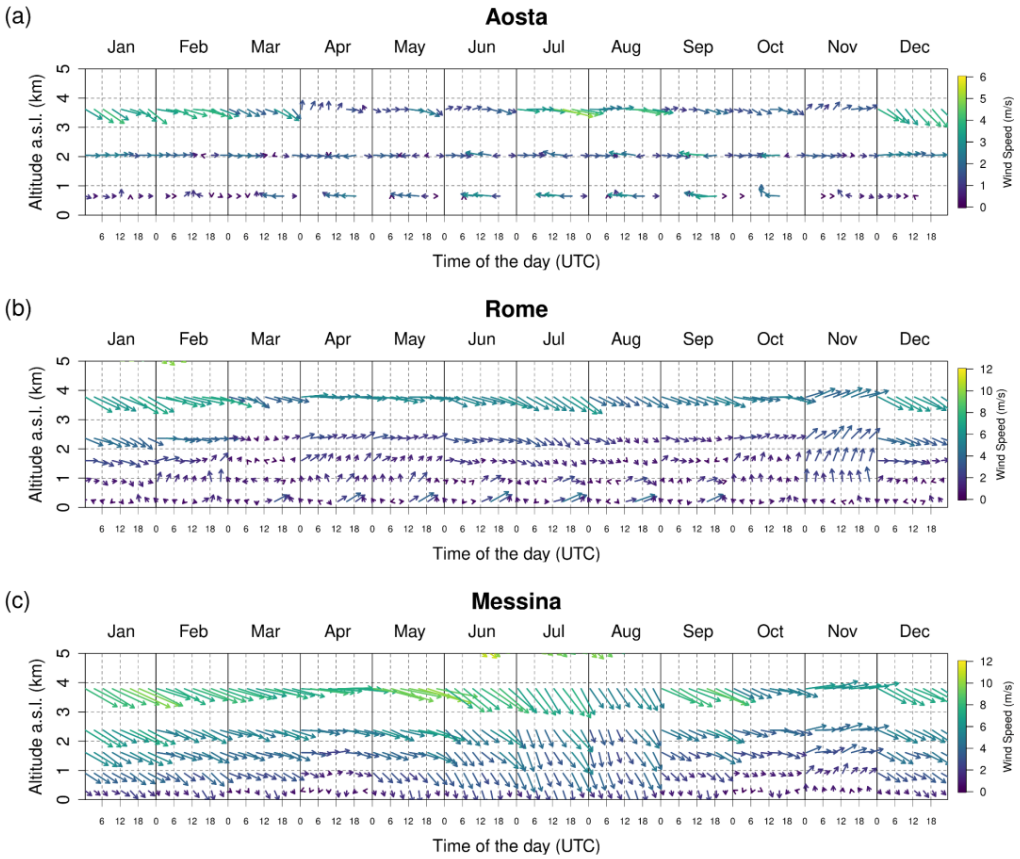


Figure 5. Monthly and daily resolved median (2016–2022) horizontal winds from the (**a**) MERIDA and (**b**,**c**) ERA5 reanalysis, plus surface wind from meteorological measurements at the first vertical level. Note the different wind speed colour scale in Aosta with respect to Rome and Messina.

A first comparison between the ALC and CAMS data is performed in Figure 6, showing the seasonal statistics of ALICENET's PM retrievals and the CAMS model's PM_{10} outputs. The ALICENET data are reported both as ambient total PM concentrations and after adjustment to dry conditions using hygroscopic correction (see Section 2.2). As a further comparison, we include the PM_{10} measurements from EPA air quality monitoring stations (Table 1), these referring to dry conditions as per standard protocols. All the statistics refer to the period 2018–2022. The hygroscopicity-corrected ALICENET estimates at ground level typically align within 30% of the independent EPA measurements, consistent with previous validation studies [43]. An expected exception occurs in Aosta during winter, when the strong temperature inversions trap particles below the ALC detectable range (<200 m) and when the difference between local emissions at the urban EPA and the semi-rural ALICENET stations becomes significant. For further insights, we include in Appendix A.2 a monthly resolved comparison between the in situ PM_{10} measurements (dry) and our wet/dry ALC-based PM estimates (Figure A3). This is intended to further highlight the important effects of particle humidification on the PM in 'real world' conditions (such as those reported in Figure 4). This helps us to understand, for example, that some summer decrease in the ALC PM in the lowermost levels is not only related to decreased emissions from some sources (e.g., heating) and increased aerosol mixing but is also due to the lower ambient relative humidity and thus less particle aqueous processing in the atmosphere.

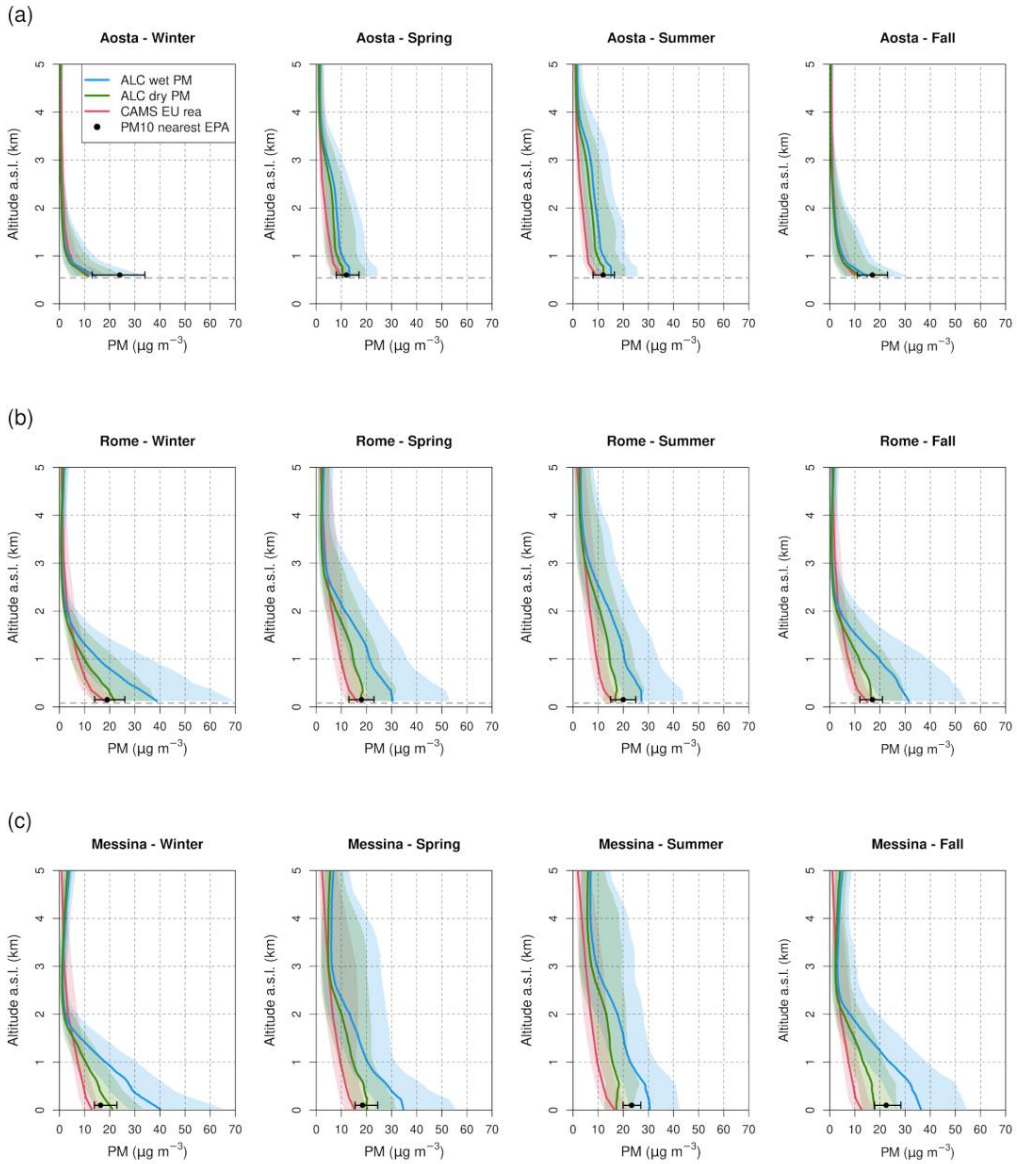


Figure 6. Seasonal median values (lines) and interquartile ranges (shaded area) of the wet (light blue) and dry (green) ALICENET PM estimates and the CAMS PM_{10} data (red) in (**a**) Aosta, (**b**) Rome, and (**c**) Messina. The relevant statistics of the surface PM_{10} concentrations measured by the nearest EPA station (black dots) are also reported. The addressed period is 2018–2022.

The model–observation comparison reveals that CAMS exhibits good agreement with the ground-level PM_{10} measurements (as expected, given the model assimilation of these data). However, the CAMS PM_{10} concentrations remain consistently lower than the relevant dry ones retrieved from ALC observations in the first 2 km, with the winter conditions in Aosta being the sole exception. Within this vertical range, the CAMS data also exhibit reduced variability compared to ALICENET and, in some cases, a different vertical profile shape. Such a CAMS underestimation tendency aligns with previous evaluations against vertically resolved measurements (e.g., [37]). Above a 2 km altitude, the CAMS outputs generally show better agreement with the ALICENET PM retrievals.

Figure 7 provides a deeper examination of the ALC–CAMS differences, illustrating the monthly and daily resolved median differences between the CAMS PM_{10} and the ALC-based dry PM in the 0–5 km vertical range. This daily resolved analysis highlights certain model limitations in reproducing the observed vertical development of diurnal dynamics. Specifically, the model inadequately captures the recurrent advection of polluted

air masses from the Po Valley to Aosta (Figure 7a) and the intensity of convective mixing in Rome (Figure 7b), both processes significantly influencing the surface PM concentrations. Figure 7 also shows that in Messina, the CAMS data better align with ALICENET in the first few hundred metres during the central hours of the day (Figure 7c), contrasting with the patterns observed in Rome. Nevertheless, negative biases exceeding 10 μg m^{-3} persist at both southern sites, as is particularly evident in Messina's March profiles below 800 m.

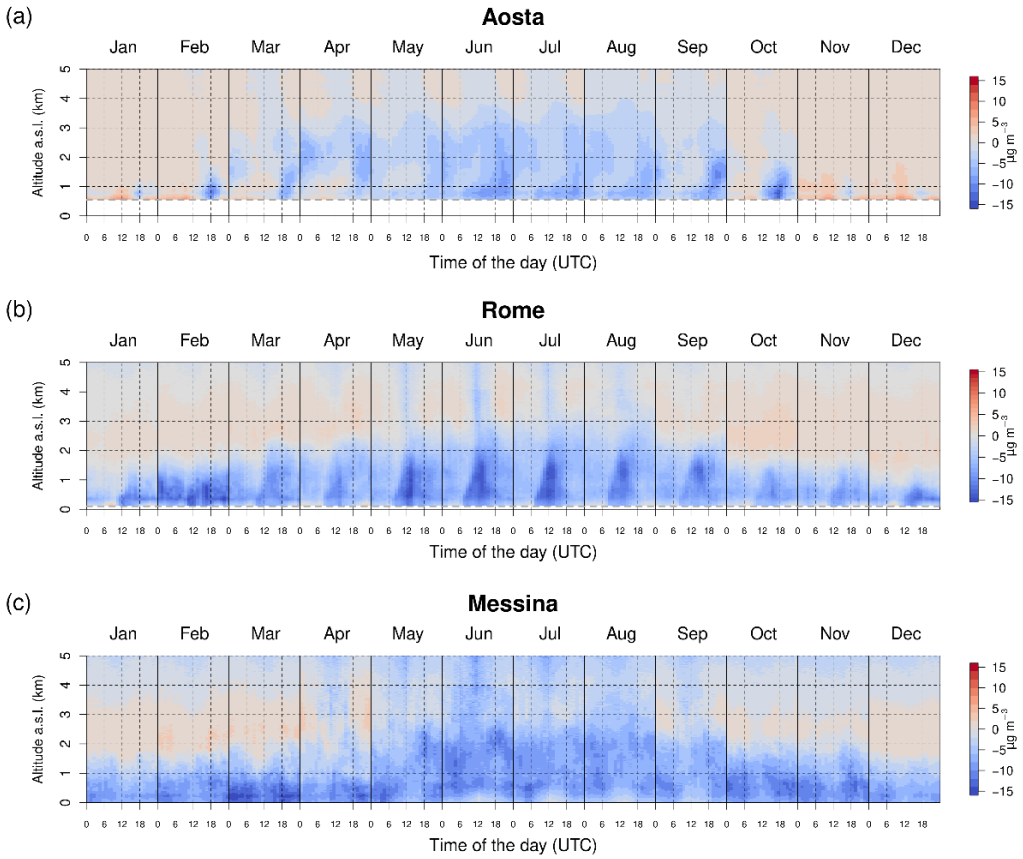


Figure 7. Median differences between the CAMS PM_{10} data and the ALICENET dry PM estimates in (**a**) Aosta, (**b**) Rome, and (**c**) Messina. The addressed period is 2018–2022.

3.2. Vertical Build-Up of Aerosol Optical Depth and Diurnal–Nocturnal Variability

Based on the 7-year ALICENET datasets of the aerosol extinction profiles, we derived the monthly and daily resolved median values of the columnar AOD and its vertical build-up along the atmospheric column.

The results are given in Figure 8, showing the total AOD (black dots) and the vertically resolved AOD percentage (colour scale), defined as:

$$\mathrm{AOD\%(z)} = \frac{\int_0^z \alpha(z', t)\mathrm{d}z'}{\mathrm{AOD}} 100 \quad (3)$$

where α represents the ALICENET-derived aerosol extinction coefficient at 1064 nm, and the altitude, z, ranges between 0 and 5 km.

This view reveals the altitude ranges where most of the AOD resides, showing marked seasonal and daily variability. During winter months, strong atmospheric stability confines aerosols primarily to the lower atmospheric levels. In contrast, the spring and summer periods exhibit increased aerosol loading in the free troposphere, driven by enhanced photochemistry and convection [75]. At shorter timescales, vertical mixing uplifts particles during daytime hours, while particle formation and growth processes during nighttime and early morning can enhance the aerosol concentrations aloft [23].

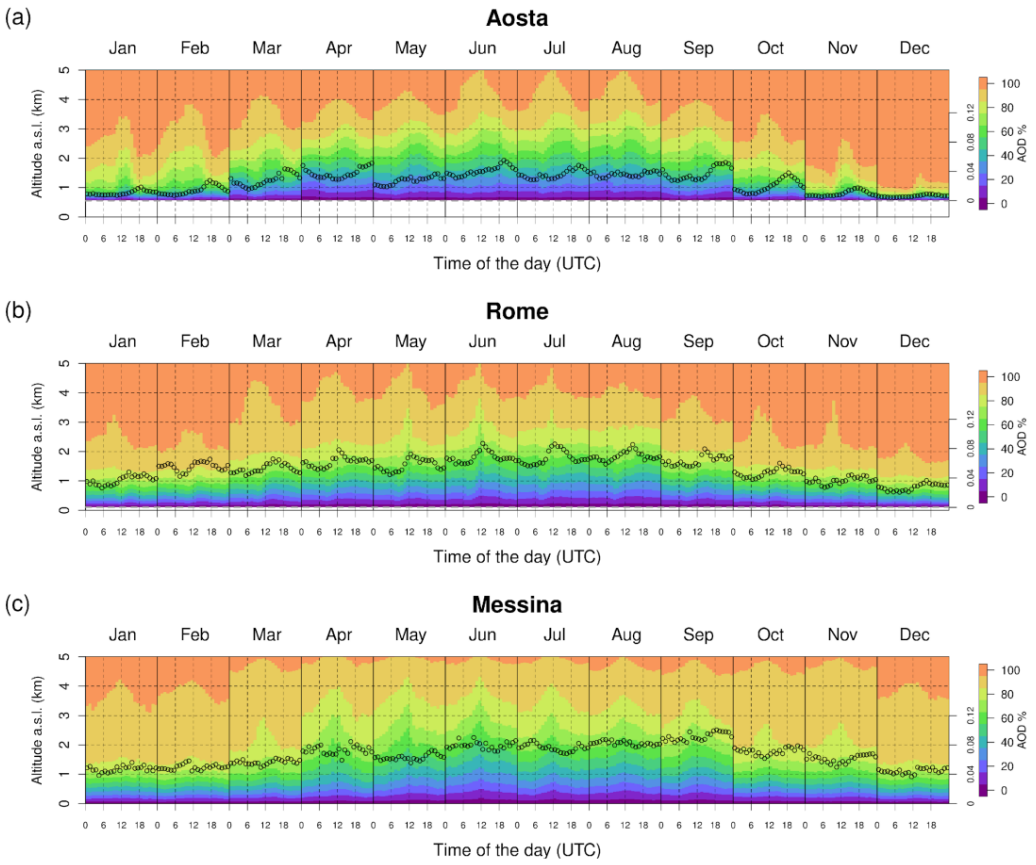


Figure 8. Median value (2016–2022) of the ALICENET-derived AOD (at 1064 nm, black dots, right y-axis) and relevant vertical build-up from ground level to a 5 km altitude (in percentage, colour scale) in (**a**) Aosta, (**b**) Rome, and (**c**) Messina.

These dynamics translate into substantial contributions from the lower troposphere to the total AOD, particularly in highly urbanised environments like Rome, where local anthropogenic emissions play a significant role. Specifically, in Rome, approximately 70% of the total AOD resides in the first kilometre during winter, while in summer, this same contribution extends above a 2 km altitude. At the Alpine site in Aosta, despite its weaker local sources, up to 80% of the AOD resides in the first kilometre during January and December due to the strong atmospheric stability conditions. During summer, over 30% of the AOD is built above 2 km a.s.l. across the study sites, with Messina showing the maximum contribution of 40% from these upper layers. These results are consistent with previous studies on the aerosol vertical distributions in the Po Valley [76] and other European areas [77].

The continuous operation of ALC enables comparison between the diurnal and nocturnal AOD, thus complementing the day-only AERONET/SKYNET sunphotometer data or polar orbit satellite-based information. In this respect, Figure 9 presents a monthly resolved comparison of the diurnal (between sunrise and sunset hours at each site) and nocturnal ALICENET-derived AOD. Overall, the nocturnal–diurnal AOD difference remains mostly below 15%, with site-specific characteristics. In Rome, the nocturnal AOD values generally fall below diurnal levels, attributable to the nighttime sea–land breeze circulations enhancing particle removal [48]. Conversely, Messina exhibits generally higher nocturnal AOD values compared to daytime, likely due to enhanced hygroscopic marine particle growth. These aspects will be further explored through the availability of AERONET lunar photometry, whose retrievals are currently in a test phase [78] at some ALICENET sites (including Rome and Aosta).

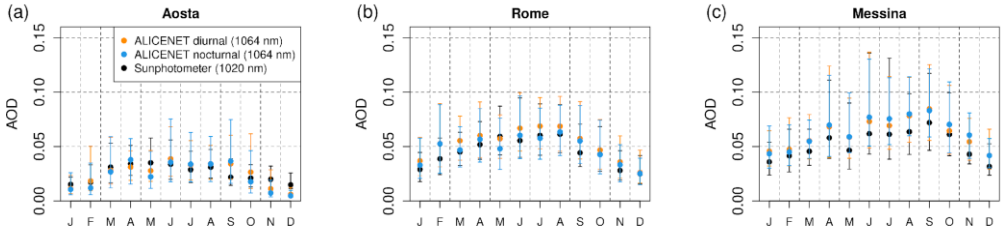


Figure 9. Monthly median values and interquartile ranges (bars) of the diurnal (orange dots) and nocturnal (blue dots) ALICENET-retrieved AOD in (**a**) Aosta, (**b**) Rome, and (**c**) Messina during 2016–2022. The corresponding AOD statistics from the nearest AERONET or SKYNET sunphotometer are also displayed (black dots).

3.3. Aerosol Vertical Layering and Investigation of Main Driving Factors

ALICENET's ALADIN algorithm enables the automatic detection of aerosol layers from ALC observations. As described in Section 2.2, this tool provides continuous, high-resolution data on the height and vertical extent of key aerosol structures, namely the mixed and continuous aerosol layers (MAL and CAL) and elevated aerosol layers (EALs). In the following, we present the statistics of the layering information derived from the 7-year ALC observations and integrate it with relevant data from state-of-the-art models.

Figure 10 illustrates the monthly and daily resolved median values of the MAL and CAL heights. The MAL exhibits pronounced diurnal variability, primarily driven by turbulent mixing, and distinct characteristics across the study sites. In Aosta, the valley compensating flows [79] contribute to suppressing MAL development, resulting in heights of around 500 m in winter and 1.3 km in summer. Note that in Aosta, the MAL is a better indicator of vertical mixing development compared to the PM fields in Figure 4. In fact, the ALADIN's MAL detection relies on vertical correlations rather than on absolute PM values, with these being also significantly influenced by horizontal mesoscale advections.

Rome's data display mixed layer evolution typical of urban areas [80], with rapid growth during the morning, reaching heights exceeding 2 km in summer. In Messina, the coastal setting leads to a distinctly different pattern, with a relatively shallow mixed layer year-round due to the stabilising influence of the sea, which suppresses vertical mixing as detected by lidar techniques in other Italian coastal sites [81].

The CAL variability is mainly seasonal, with the higher values in spring–summer associated with the enhanced background aerosol concentrations resulting from convection and photochemical aerosol production [75], as well as the higher frequency of natural and anthropogenic aerosol transport events in the middle troposphere. The CAL in Aosta features marked increases from winter to summer months (from 1.5 to 4 km a.s.l.) attributed to enhanced local circulations (e.g., slope winds, [82]) and regional transport of polluted air masses from the Po Valley in the afternoon [21], resulting in significant daily fluctuations. In contrast, the CAL in Rome demonstrates greater stability, exceeding 2 km a.s.l. even during winter months. This is ascribed to the higher aerosol concentrations in the urban environment and generally lower atmospheric stability, facilitating deeper mixing of pollutants. The CAL in Messina displays the highest variability among the sites, reaching altitudes of >4 km during summer. This primarily results from frequent intrusions of Saharan dust-laden air masses in the Southern Mediterranean [72], as discussed in the following.

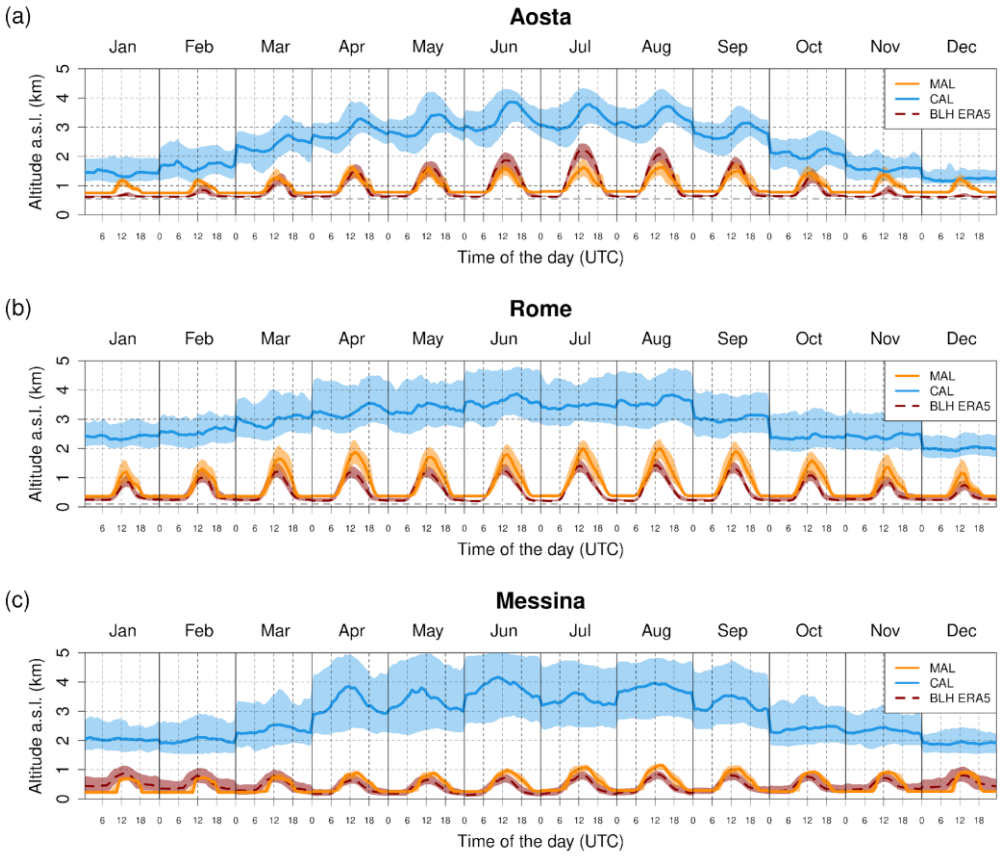


Figure 10. Median values (2016–2022) and interquartile ranges (shaded areas) of the CAL and MAL in (**a**) Aosta, (**b**) Rome, and (**c**) Messina.

An intriguing feature observed at all the sites is the discontinuity in the CAL at the beginning of spring and autumn (February–March and October–November). This pattern likely reflects the transition between dominant meteorological regimes, such as the shift from stable winter conditions to more convective summer patterns and vice versa.

In Figure 10, we also compare the ALC-based MAL dataset with the ERA5 boundary layer height (BLH) dataset, which is widely employed in air quality assessments. The comparison reveals good agreement between the observational and model-based approaches. Slight discrepancies are observed in the timing of the mixed/boundary layer development (e.g., in Rome) and in the estimation of its maximum extent (e.g., in Aosta, as expected due to its highly complex orography). Differences between the MAL and the BLH also stem from the distinct methodological approaches: ALICENET derives the MAL using aerosols as tracers, while ERA5 determines the BLH using a bulk Richardson number method [57].

To examine the characteristics of the elevated aerosol layers detected by the ALADIN tool across the study sites, we report in Figure 11 the monthly and altitude-resolved 7-year statistics of the EALs in terms of the occurrence frequency (left panels) and average PM contribution (right panels).

For each month (m) and altitude bin (z), we define the EAL frequency of occurrence as:

$$\text{frequency}(m, z) = \frac{N(m, z)}{Ntot} \quad (4)$$

where N(m,z) represents the number of time intervals when EALs are detected within month m at altitude z, and Ntot is the total number of observation intervals in that month.

To quantify the typical impact of these layers on the aerosol loading, we derive their average PM contribution as:

$$\text{EAL average PM contribution}(m, z) = \frac{\sum_j \text{PM}(j, z)}{N(m, z)} * \text{frequency}(m, z) \quad (5)$$

where PM(j,z) represents the ALICENET-derived PM concentration at altitude z during the j-th EAL-affected time interval.

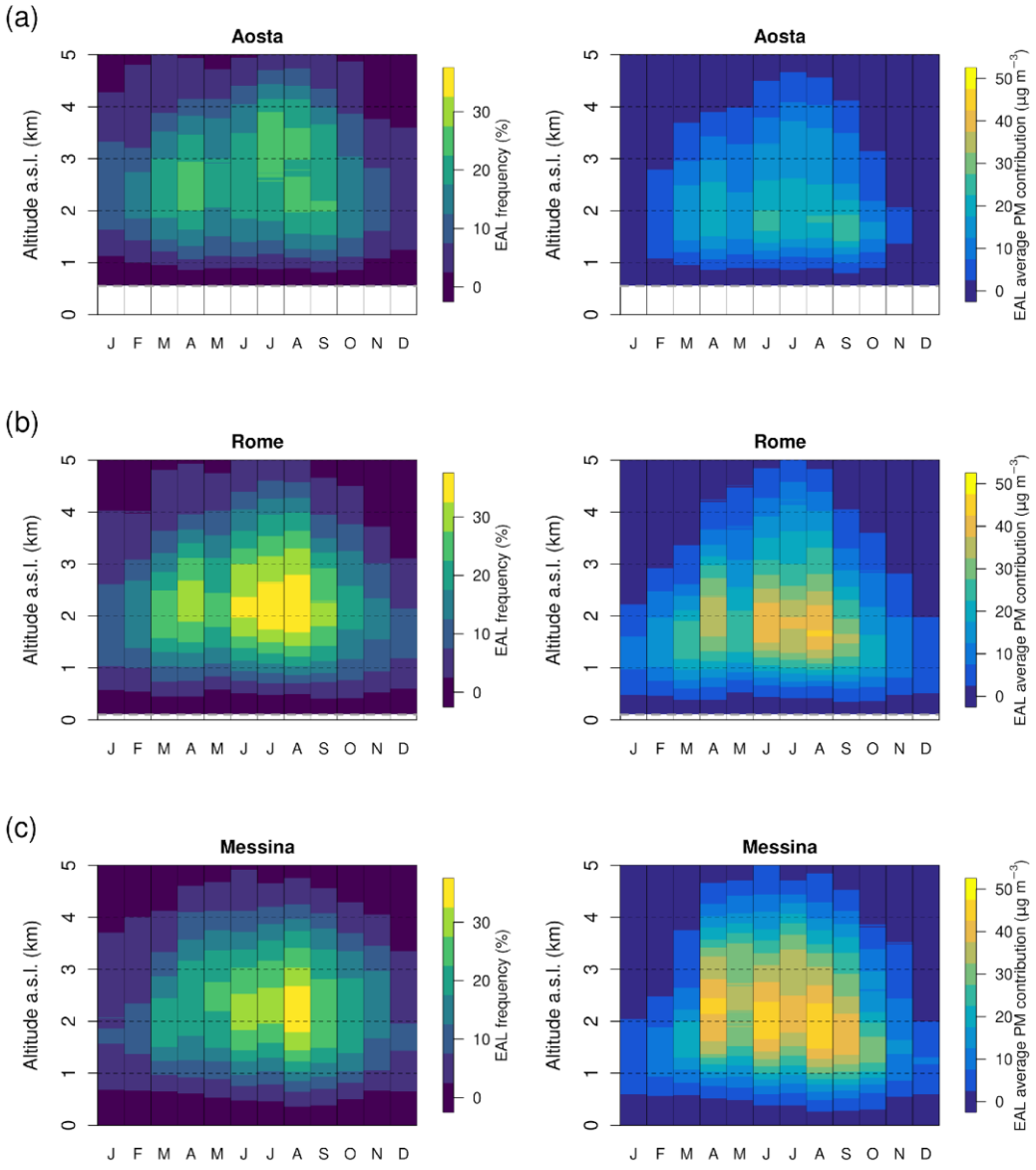


Figure 11. Monthly and altitude-resolved frequency of occurrence (left panels) and average contribution to the PM concentrations (right panels) of the EALs detected by ALICENET over (**a**) Aosta, (**b**) Rome, and (**c**) Messina (2016–2022).

Figure 11 reveals marked latitudinal and seasonal variability in the EAL characteristics. The central Mediterranean sites exhibit particularly high EAL occurrence during the summer months, when these layers are present more than 30% of the time between a 2 and 4 km altitude. The impact on the PM concentrations is most significant below 3 km, where the summer values in Rome and Messina can reach up to 45 μg m^{-3}.

This spatiotemporal variability reflects the diverse influence of non-local aerosol sources and transport mechanisms across Italy. At the northern site of Aosta, the aerosol

stratification primarily results from anthropogenic emissions and mesoscale circulations within the Po Valley [20]. In summer, this location experiences long-range transport of biomass-burning plumes traversing the Atlantic, a phenomenon frequently documented over Northern Europe [83]. In contrast, Rome and Messina are mainly influenced by Mediterranean synoptic-scale transport patterns, particularly mineral dust intrusions from North Africa and Eastern Europe [19,72,84–86]. These southern sites receive additional contributions from biomass-burning plumes of varying transport distances [87,88], marine aerosols [89], and occasional volcanic ash plumes [90].

A common feature across all the sites is the April peak in the EAL frequency, corresponding to the relative AOD maximum shown in Figure 9. Satellite data analysis has attributed this enhancement to agricultural burning activities in Eastern Europe [88]. Our work further characterises the vertical ranges affected by this phenomenon. Additionally, non-negligible PM contributions emerge during September–October, attributed primarily to low-altitude Saharan dust intrusions towards the central Mediterranean [91].

To investigate the meteorological conditions associated with the observed EALs, we analysed the ERA5 geopotential heights at 500 hPa during the ALICENET-detected EAL events. Figure 12 shows the resulting geopotential anomalies relative to the mean seasonal conditions for winter (left panels) and summer (right panels). The corresponding mean geopotential fields during the EAL events are provided in Appendix A.2 (Figure A4). This analysis revealed distinct seasonal patterns that strongly influence the aerosol transport pathways in the Mediterranean region.

During winter, a prominent trough over the west–central Mediterranean characterises the EAL events in Rome and Messina. This trough, associated with cyclonic systems, facilitates meridional dust transport into the Mediterranean basin. The corresponding negative geopotential anomalies indicate trough intensification, enhancing the cyclonic activity and southerly flows transporting desert dust to Southern Europe [91,92]. Concurrently, the positive anomalies northeast of the Mediterranean suggest a blocking high-pressure system, further channelling dust into the region at lower tropospheric levels.

The summer patterns feature a robust ridge from North Africa into Southern Europe, associated with the Saharan high. The resulting pressure gradient drives northward dust transport [93,94], while the positive geopotential anomalies centred over the study sites can lead to stronger subsidence and prolonged stagnation periods.

The Alpine site of Aosta exhibits distinctive synoptic patterns during the EAL events. In winter, high-pressure conditions dominate over northern Italy, primarily associated with aerosol stagnation in the Po Basin. Analysis of the transport mechanisms reveals a vertical decoupling for this site (Appendix A.2, Figure A5): while EALs below 2.5 km form under these stagnant conditions [95], those above 2.5 km develop within cyclonic configurations similar to those observed in Rome and Messina.

In summer, the persistent high-pressure conditions over Central Europe support thermally driven winds that transport aerosols from the Po Basin through plain-to-mountain breezes [21].

Focusing on the potential impacts of the EALs on air quality, we investigated their effects on the PM concentrations within the MAL and, in turn, at the ground level. Such effects can arise from direct contributions to the surface PM levels via entrainment of the EALs into the mixed layer [41], as well as through increased atmospheric stability caused by long-range transport of warm air, rich in absorbing aerosols, potentially exacerbating surface pollution [96].

Based on our 7-year statistics, Figure 13 shows the monthly resolved number of days affected by the EALs (green bars). More specifically, a day was classified as EAL-affected if an elevated aerosol layer was detected for at least one hour. The frequency

of EAL-affected days exceeds 60% during the summer months across all the study sites, though with differing temporal patterns. Aosta experiences its peak in July–August, while Messina shows maximum frequency in August–September. Rome exhibits a more uniform distribution over the year.

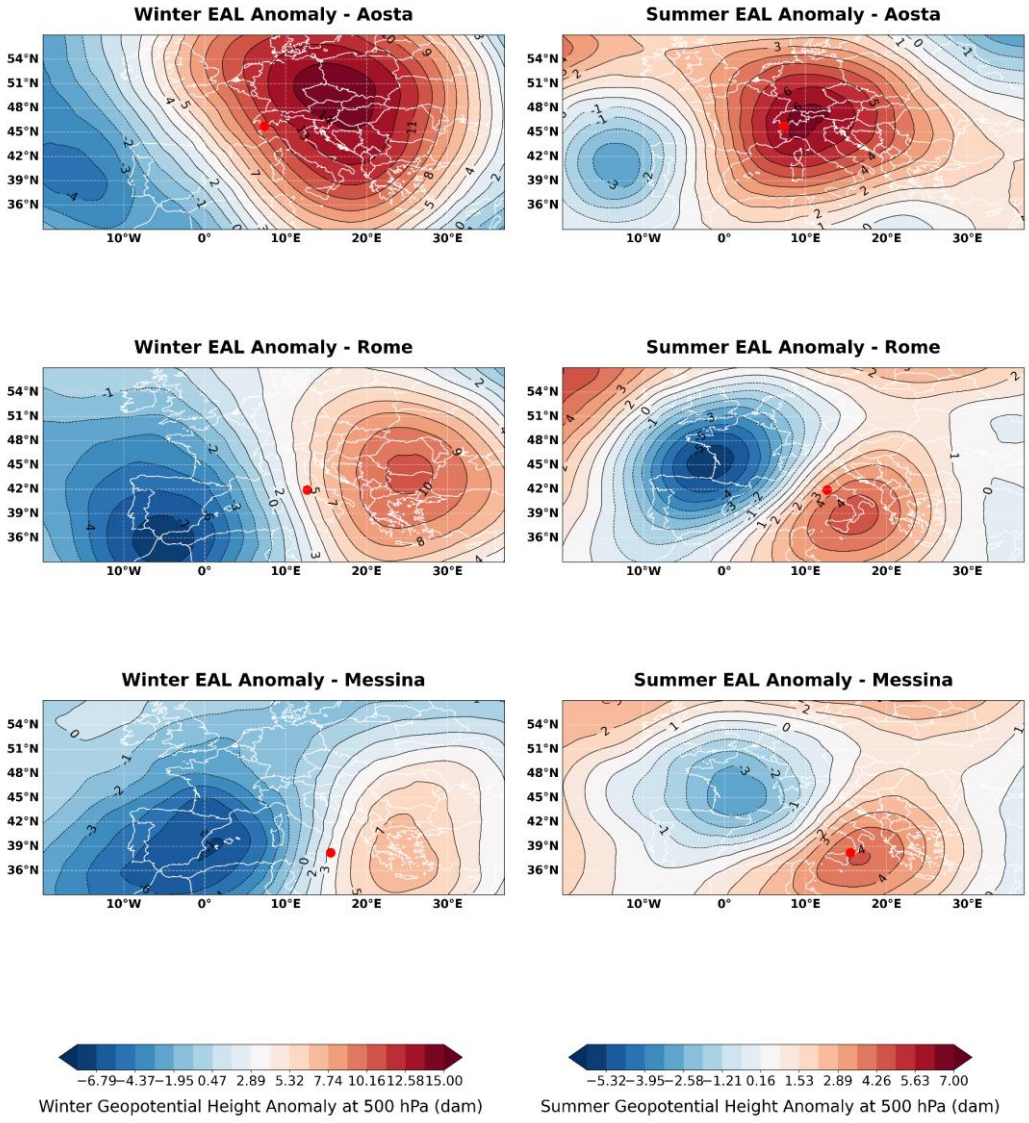


Figure 12. The mean (2016–2022) 500 hPa geopotential anomalies (ERA5 fields) relative to the mean seasonal conditions during the ALICENET-detected EAL events in winter (**left column**) and summer (**right column**) over (from top to bottom) Aosta, Rome, and Messina (red dots).

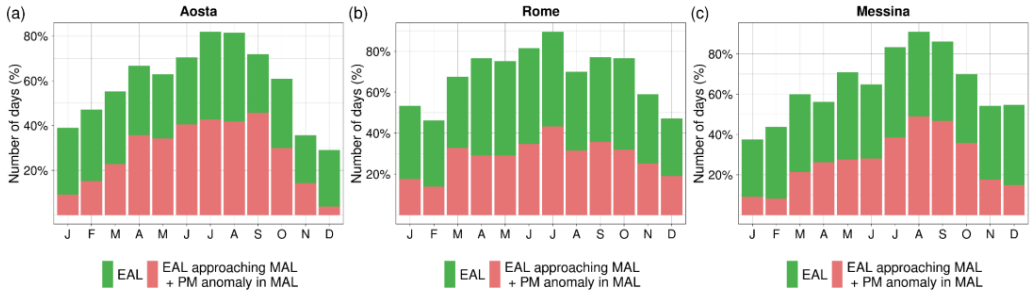


Figure 13. Monthly resolved frequency of days with EALs detected by ALICENET (green bars) and subset statistics (red bars) of those EAL impacting the MAL PM loads (see text) over (**a**) Aosta, (**b**) Rome, and (**c**) Messina during 2016–2022.

A subset of EAL-affected days was then derived by selecting the days in which (a) the EAL approaches the MAL upper boundary (<500 m distance), and (b) the MAL PM concentrations exceed the site-specific reference ones derived from the long-term ALC dataset (see Figure 6). Our results reveal that, depending on the month, 10–40% of EAL-affected days also register enhanced levels of PM within the mixed layer. Most of these cases can be attributed to Saharan dust transport, particularly in central and southern Italian sites [41]. Further investigation of this aspect will be performed in the future through recently integrated polarisation-sensitive ALC systems (PLCs) within the ALICENET network [43]. In fact, these systems offer enhanced capabilities for distinguishing irregularly shaped particles, such as mineral dust, from spherical ones typical of anthropogenic origin.

As long-term PLC observations are not yet available, to assess the composition of the detected EALs, we exploited aerosol speciation data from CAMS, focusing on the dust and wildfire PM_{10} components (Section 2.3). As an initial step, we compared the total PM_{10} CAMS concentrations with the ALICENET-derived PM concentrations during the EAL events (2018–2022). As expected from previous results (e.g., Figure 6), this comparison revealed CAMS's negative biases with respect to ALICENET, with the EAL mass concentration differences generally being <30 μg m^{-3} (see Appendix A.2, Figure A6). The most substantial differences emerged in cases of heavily loaded aerosol layers (i.e., ALC-based PM > 80 μg m^{-3}) or thin layers that the model's coarse vertical resolution failed to resolve.

To ensure meaningful interpretation of the ALC-detected EALs based on the CAMS model data, we thus restricted this analysis to episodes where the difference between the ALC and CAMS mass concentrations within the EAL remained below 30 μg m^{-3}. For these cases, we classified each EAL as dominated by particulate matter of desert dust (PM_{10}DUST), wildfire (PM_{10}WF) or other PM_{10} origins (PM_{10}OTHER = PM_{10}TOT − PM_{10}DUST − PM_{10}WF), depending on which CAMS species most significantly exceeded its seasonal median profile within the relevant EAL vertical range and affected time window. The seasonal median profiles used as references for the CAMS PM_{10}DUST, PM_{10}WF and PM_{10}OTHER are reported in Appendix A.2 (Figure A7).

The results of this combined ALC–CAMS analysis are summarised in Figure 14. This analysis complements the results in Figure 11 by characterising the aerosol type of the ALC-detected EAL based on the CAMS species.

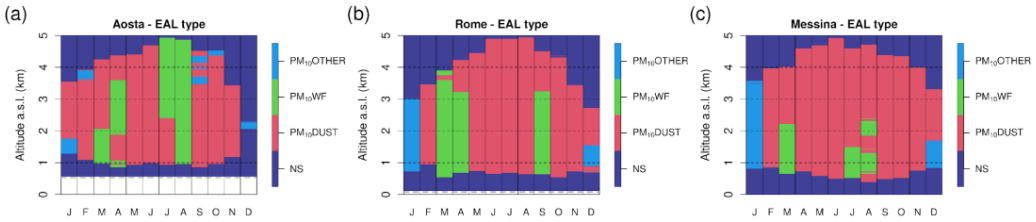


Figure 14. Monthly and altitude-resolved statistics (2018–2022) of the dominant aerosol type (desert dust, wildfires, others) identified through CAMS data in correspondence to the EALs detected by ALICENET in (**a**) Aosta, (**b**) Rome, and (**c**) Messina. Dark blue indicates regions not statistically significant (NS) for EAL classification.

Figure 14 reveals desert dust to be the predominant component of the EALs throughout the year across the study sites. During winter months, CAMS indicates significant contributions from other aerosol species, most likely particles of more local origin suspended above the MAL. The wildfire component becomes more pronounced in spring and summer, reflecting both local and long-range transported biomass-burning plumes [83,88]. This seasonal pattern is particularly evident over Aosta during July–August. However, as already pointed out, the absolute PM_{10}WF concentrations reconstructed by CAMS remain consistently low, with median seasonal values of <0.1 μg m^{-3} (Appendix A.2, Figure A6).

Such remarkably low values could be attributed to either incomplete wildfire emission inventories in the CAMS dataset used here or the model's inability to resolve thin wildfire plumes due to its coarse spatial resolution.

4. Discussion

The statistical analysis of the observational and model-based aerosol profiles across Italy performed here showed distinct daily and annual cycles in the aerosol vertical distributions, revealing interplays between local sources, mixing processes, mesoscale circulations, and large-scale transport dynamics. Overall, marked latitudinal and environment-related differences emerged.

At the Alpine site of Aosta, the median PM concentrations remained mostly below 15 $\mu g\ m^{-3}$ during the year and along the vertical profile. Winter conditions showed strong atmospheric stability, which confined aerosols to the lowest atmospheric levels, resulting in MAL heights below 500 m and concentrating up to 80% of the total AOD within this layer. The upper atmospheric layers were significantly impacted by mountain–valley breezes acting at the regional scale. These breezes systematically transported aerosol-laden air masses from the Po Valley during the afternoon, reaching maximum layer heights of 4 km a.s.l. and PM loads up to 20 $\mu g\ m^{-3}$ between a 1 and 2 km altitude during summer months, confirming and extending previous findings [21].

The Rome site exhibited characteristics typical of major urban Mediterranean environments. The median PM in the first kilometre exceeded 30 $\mu g\ m^{-3}$ (more than double the Aosta values) all year round, though with marked daily-to-seasonal modulations. These were shaped by vertical mixing processes, with the MAL reaching above 2 km in summer, and local circulations, with land–sea breezes removing up to 35% of the aerosol load in the afternoon.

In the coastal Messina site, local aerosols of both natural and anthropogenic origin remained mainly confined within a 1 km thick MAL throughout the year, observationally confirming the stabilising influence of the marine boundary layer. These results underscore the utility of vertically resolved observations in complex geographical settings and the critical role of atmospheric dispersion dynamics in determining local air quality.

Regarding the optical properties, significant seasonal and latitudinal gradients emerged across Italy. Maximum contrast was found between the southern Italy summer conditions and the northern Italy winter ones. In fact, the percentage of the AOD built within the first 1000 m in altitude ranged between 30% (Messina, summer) and 80% (Aosta, winter) of the total column AOD. In terms of the diurnal variability, the AOD cycle showed day–night variations of about $\pm 15\%$, with the nocturnal values lower in Rome due to sea breeze particle removal and higher in Messina due to hygroscopic particle growth. This AOD information complements the daytime-only observations provided by sunphotometers and satellites.

Above the MAL, our results highlighted the frequent presence of elevated aerosol layers in the mid-troposphere, particularly in central–southern Italy (Rome and Messina). In spring and summer, the frequency and vertical extent of these layers reach their maximum, with EALs between 2 and 4 km in altitude detected over 30% of the time. In general, the PM contributions associated with the EALs maximise in the altitude range 1–3 km a.s.l., increasing southward and reaching concentrations exceeding 40 $\mu g\ m^{-3}$ at the Rome and Messina latitudes. The nearly ubiquitous presence of EALs in the spring-to-summer Mediterranean mid-troposphere translates into 40% of the AOD being built above 2 km across all the sites, peaking at 60% in Messina. This demonstrates the significant influence of regional background aerosols and long-range transport processes on the total column aerosol load.

Our analysis also revealed significant interactions between the EALs and the MAL and, thus, the surface air quality. In fact, on 10–40% of days across the study sites, the presence of an EAL close to the MAL upper boundary was associated with increased PM concentrations within it. This result underscores the capability of ALCs to complement in situ data in detecting elevated layers affecting local air quality, supporting the attribution of PM exceedances and the design of targeted mitigation strategies [11].

Through the integration of the ALC profiles with ERA5 and CAMS model reanalysis data, we found that the ALC-detected EALs were mainly associated with the transport of desert dust from North Africa and biomass-burning plumes of different origins. Characteristic synoptic patterns associated with EAL events emerged: winter troughs facilitated meridional dust transport, while summer ridges enhanced direct transport across the Central Mediterranean. The combined analysis of the ALICENET and CAMS data indicated desert dust to be the dominant component of the EALs in terms of both the frequency and the load at all the sites. CAMS also suggests a non-negligible frequency of wildfire-related EALs in spring and summer, particularly in northern Italy. This is attributed to the transport of biomass-burning plumes across the Atlantic, also frequently detected in Northern Europe. However, in quantitative terms, the wildfire-associated PM_{10} concentrations in the CAMS data appear very low. In Messina, the CAMS median seasonal value of the wildfire PM_{10} keeps below 0.1 $\mu g\ m^{-3}$ despite the fire-prone climatic conditions of southern Italy. This suggests a possible underestimation of the local and/or regional wildfire emissions in the CAMS ensemble dataset and insufficient vertical resolution to capture thin wildfire plumes. As a future plan, the relative contribution of wildfire and desert dust transport to EAL loads will be further investigated through recently integrated polarisation-sensitive ALC measurements within ALICENET, enabling discrimination between irregular dust particles and typically spherical biomass-burning ones [19].

Concerning the lowermost aerosol stratifications, the statistics of the ALC-derived MAL heights at the three sites were found to match well with the relevant statistics of the ERA5 BLH. The differences in the MAL and BLH daily cycles ranged from 10% to 35%, with major discrepancies registered for Aosta. These are attributed to the different spatiotemporal resolutions and methodological approaches used to infer these parameters within ALICENET (aerosol-based MAL) and ERA5 (thermodynamics-based BLH), which become more critical over complex terrain such as the Alpine Aosta one. In fact, a specific ERA5 vs. measurements comparison performed here for the surface wind fields showed good agreement in Rome and Messina, and reduced agreement in Aosta.

In terms of the PM_{10}, CAMS data are shown to reproduce the values well at the surface level (as expected, given the assimilation of the measured PM_{10} data from air quality monitoring networks into the model reanalysis). Along the vertical profile and up to a 2 km altitude, the CAMS values are found to be 5–15 $\mu g\ m^{-3}$ lower than our ALC-based retrievals, particularly at southern Mediterranean sites.

The reliability of these results is supported by careful consideration of the instrumental and model uncertainties and comparison with independent measurements, as detailed in Section 2. For the ALCs, we estimate a maximum uncertainty of 30–40% for the aerosol extinction and up to 50% for the mass concentrations, although systematic comparisons performed in previous studies demonstrate better performances [43].

Overall, even taking into account the uncertainties in both the measurement-based and model-based data, this effort indicates some statistically significant discrepancies in the CAMS-modelled PM_{10} with respect to the ALICENET PM product. These can be summarised as a model underestimation of the PM (5–15 $\mu g\ m^{-3}$) within the MAL, and a still-lacking representation of the PM diurnal dynamics (mixing and mesoscale fluxes) along the vertical dimension.

5. Conclusions

The high-resolution multiannual datasets we retrieved across Italy expand current knowledge of the aerosol characteristics in the Central Mediterranean area. In fact, while vertical profiling of the aerosol optical properties in Italy was documented in previous studies, though with coarser temporal resolution and shorter temporal coverage, the datasets presented here provide novel, observation-based information on the aerosol mass vertical distributions, layering structures, and relevant latitudinal and daily-to-seasonal variability.

The presented quality-assured ALICENET dataset, made publicly available, serves multiple applications. For air quality, it provides detailed information about the PM dynamics, mixed layer heights, and allows for the estimation of the influence of elevated aerosol layers on surface air quality. For climate studies, it offers an observational record of essential climate variables (aerosol extinction and optical depth) in both daytime and nighttime conditions, with the latter being mainly unavailable based on alternative passive remote sensing. The vertically resolved, long-term nature of these observations will also help better interpret the AOD trends, disentangling changes in the near-surface and/or elevated aerosol loads.

This work demonstrates the potential of ALC networks for continuous, quantitative monitoring of aerosol vertical distributions over the long term, filling current observational gaps and enhancing our ability to improve or validate atmospheric models and satellite observations. This aligns with the objectives of major ongoing European Commission efforts, such as the H2020 RI-URBANS project and the Copernicus programme, as well as those of the ESA-EarthCARE (Cloud, Aerosol and Radiation Explorer) mission.

Author Contributions: Conceptualization, data curation, investigation: A.B. (Annachiara Bellini) and F.B.; formal analysis and software: A.B. (Annachiara Bellini) and H.D.; visualisation: A.B. (Annachiara Bellini) and F.B.; ALC instrument operations and database management: G.P.G., L.D.L., A.B. (Alessandro Bracci) and H.D.; funding acquisition and supervision: F.B.; writing—original draft preparation: A.B. (Annachiara Bellini) and F.B.; writing—review and editing: A.B. (Annachiara Bellini), F.B. and H.D. All authors have read and agreed to the published version of the manuscript.

Funding: This research received partial financial support from the European Commission (EC) H2020 Project RI-URBANS (GA No. 101036245) and from the "Agreement for Copernicus Services for the provision of CAMS—National Collaboration Programme—Italy bis Third Edition" (CAMS2_72IT_bis) funded by European Centre for Medium Range Weather Forecast (ECMWF).

Data Availability Statement: The original data presented in the study are openly available in Zenodo at the following DOI: https://doi.org/10.5281/zenodo.14419260.

Acknowledgments: Annachiara Bellini performed this work in the framework of her doctoral program in remote sensing at University 'La Sapienza' (DIET, Rome, Italy) under the scientific supervision of Francesca Barnaba. We acknowledge Annalisa Di Bernardino (University of Rome 'La Sapienza', Physics Department) for further PhD tutorship. We also acknowledge the Copernicus Atmosphere Monitoring Service (CAMS) implemented by ECMWF on behalf of the European Commission as part of the Copernicus Programme, the European Centre for Medium Range Weather Forecast (ECMWF) and 'Ricerca sul Sistema Energetico' (RSE) for, respectively, the CAMS European air quality Reanalysis ENSEMBLE data, the ERA5 Reanalysis data, and the MEteorological Reanalysis Italian DAtaset (MERIDA) used in this work. We would like to thank Michele Furnari for the support at the ALICENET site of Messina, and Gabriele Fasano for the support in the meteorological analysis of synoptic patterns in the Mediterranean region.

Conflicts of Interest: The authors declare no conflicts of interest.

Appendix A

Appendix A.1. Quality Assurance Criteria for Long-Term Analysis of ALICENET Products

To ensure the reliability and consistency of the long-term aerosol datasets analysed in this work, a set of quality assurance (QA) criteria was applied to both the aerosol profiles and layer products from the ALICENET observations. These criteria address three key aspects of data quality. First, instrument performance is verified through basic operational parameters, with the optical state metrics required to exceed 70% for data acceptance. Second, physical significance is ensured by establishing threshold values and ranges for key variables like the extinction coefficients, mass concentrations, and layer heights to filter out unrealistic values. Third, statistical robustness is guaranteed by enforcing minimum requirements for temporal coverage and data continuity to ensure representative sampling across seasons and between consecutive months.

The QA criteria are structured for two main data products. The first set applies to the aerosol profiles (QA.AP), ensuring the quality of the basic optical and microphysical retrievals. The second set addresses the aerosol layers (QA.AL), validating the detected atmospheric structures. Through these quality controls, a validated dataset of over 600,000 profiles suitable for climatological analysis was obtained, with time gaps consistently shorter than one month across the study period 2016–2022.

Table A1. Quality assurance (QA) criteria applied for long-term analysis of the ALICENET products.

ALICENET Product	QA Criteria Applied to Long-Term ALICENET Data
Aerosol Profiles (AP)	QA.AP.1 (instrument status) ALC state optics > 70% QA.AP.2 (physical significance): $0 < \alpha(z,t) < 15\ m^{-1}$, $0 < PM(z,t) < 200\ \mu g\ m^{-3}$, Std(AOD)/Mean(AOD) < 6 QA.AP.3 (statistical significance): Number of profiles/season > 10,000, Difference in data coverage between consecutive months < 30%
Aerosol Layers (AL)	QA.AL.1 (instrument status) ALC state optics > 70% QA.AL.2 (physical significance): 0 < CALH(t) < 7000 m, 0 < MALH(t) < 3500 m, $\lvert \Delta CALH/\Delta t \rvert$ < 3000 m over 3 h, $\lvert \Delta MALH/\Delta t \rvert$ < 1000 m over 1 h QA.AL.3 (statistical significance): Number of layers/season > 5000, Difference in data coverage between consecutive months < 30%

Appendix A.2. Supplementary Material for the Long-Term Analysis of Aerosol Products

Figure A1 shows the monthly and daily resolved median percentage of cloud-screened data points along the vertical dimension (0–6 km, y-axis) and across the three study sites over 2016–2022. The white-to-black colour scale indicates an increasing percentage of cloud-screened points. The percentage of cloud-screened data points varied across the study sites. In Aosta, cloud screening removed between 5% and 56% of points in the 0–6 km a.s.l. range during winter, the season most affected by cloudy conditions.

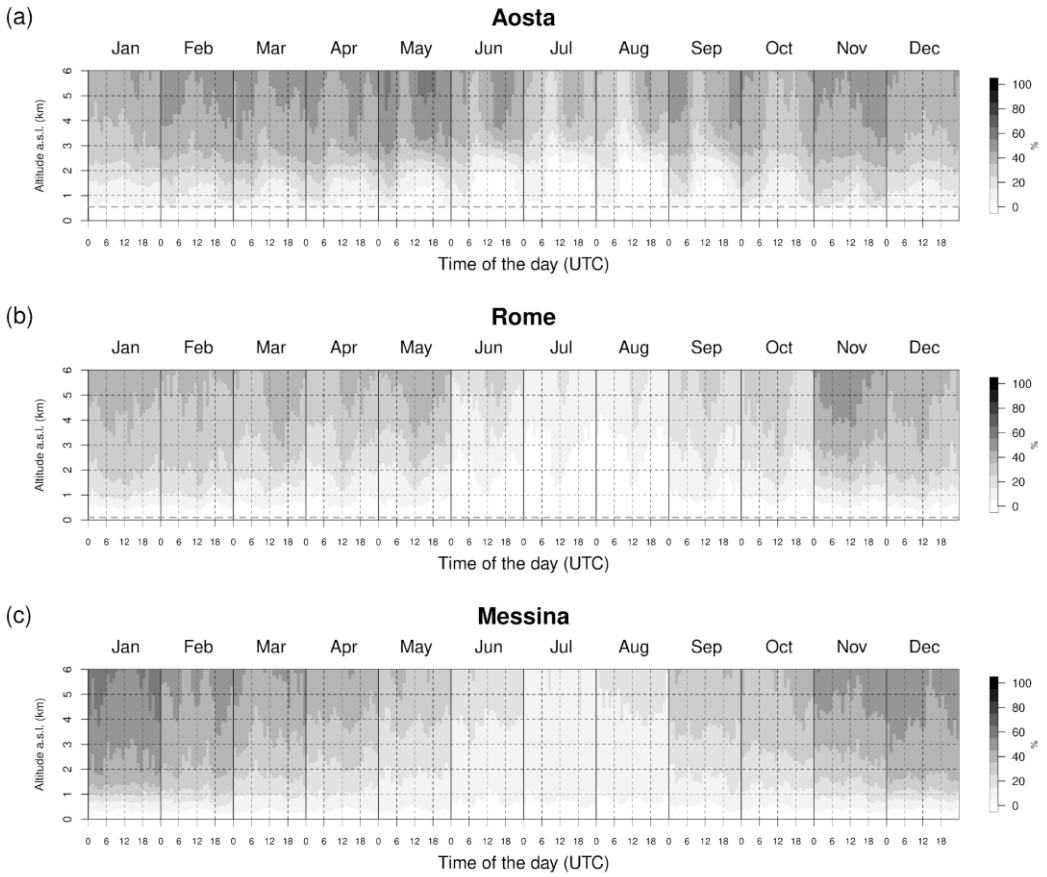


Figure A1. Monthly and daily resolved median percentage of cloud-screened data points in (**a**) Aosta, (**b**) Rome, and (**c**) Messina over 2016–2022. The grey dashed lines indicate the ground level.

Figure A2 compares the ERA5 model wind fields and the surface anemometric measurements across the study sites. The comparison reveals good agreement in Rome and Messina, where the moderately complex terrain and proximity to assimilated radiosonde measurements facilitate model accuracy. However, in the complex Alpine environment of Aosta, ERA5's coarse resolution proved insufficient to capture the observed breeze regime.

Figure A3 illustrates the monthly resolved comparison between the ALICENET PM retrievals ('real atmospheric condition' (wet) and corrected to dry PM) and the surface PM10 measurements across the three sites. The data show good agreement between the hygroscopically corrected ALC estimates and the EPA station measurements. Furthermore, a relative minimum in the wet PM concentrations in July is evident, mainly due to the lower ambient relative humidity.

Figure A4 illustrates the mean 500 hPa geopotential height fields from the ERA5 reanalysis during the winter and summer EAL events at the three study sites. The contours show the geopotential height in the dam. The maps illustrate the characteristic synoptic patterns associated with EAL occurrences: winter troughs over the Mediterranean facilitate dust transport, and summer ridges enhance north–south transport.

Figure A5 shows the ERA5 mean 500 hPa geopotential height fields during winter days with the EALs detected below and above a 2.5 km altitude over Aosta. The patterns reveal different meteorological conditions associated with low-level versus high-level EAL events at this Alpine site.

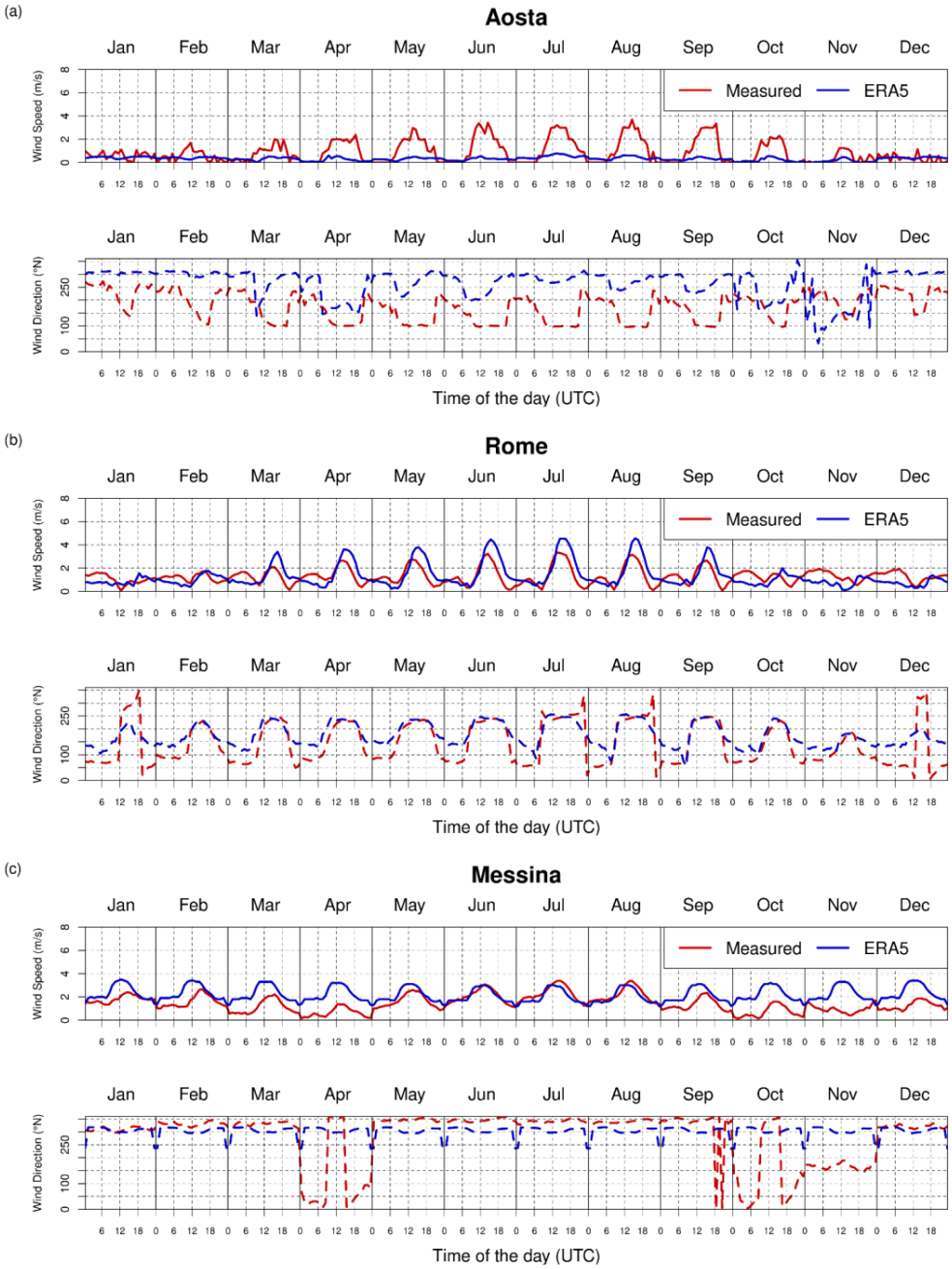


Figure A2. Monthly and daily resolved median wind speeds and wind directions at the surface level from the anemometric measurements and ERA5 reanalysis in (**a**) Aosta, (**b**) Rome, and (**c**) Messina during 2016–2022.

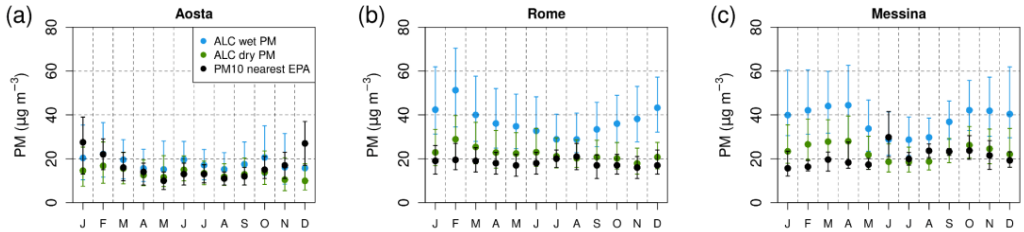


Figure A3. Monthly median values (points) and interquartile ranges (bars) of the ALICENET PM estimates ('real atmospheric condition' (wet) and corrected to dry PM) during 2016–2022 in (**a**) Aosta, (**b**) Rome, and (**c**) Messina. The corresponding statistics of the (dry) surface PM_{10} concentrations measured by the nearest EPA station are also included (black points).

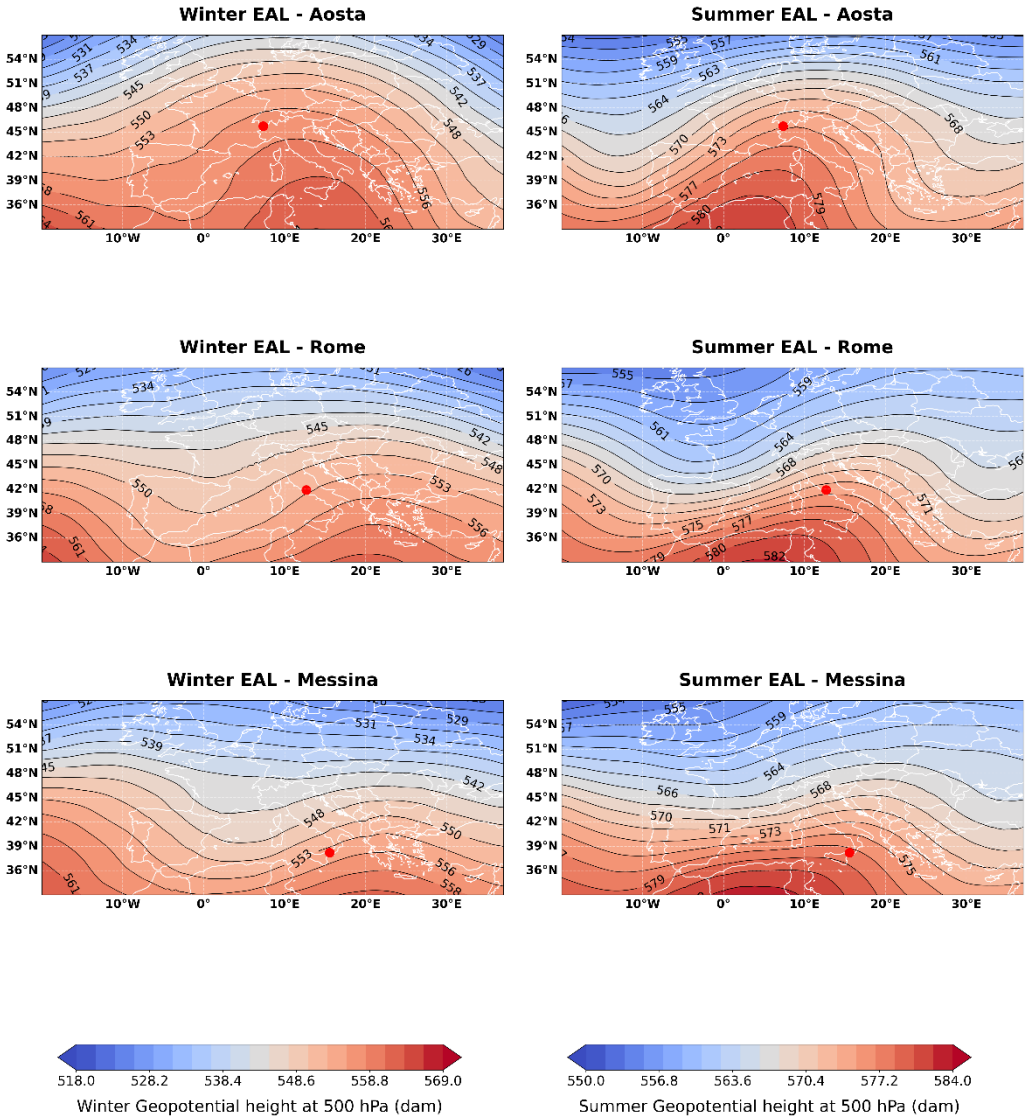


Figure A4. Mean geopotential field at 500 hPa from ERA5 during the winter (**left column**) and summer (**right column**) EAL events over (from top to bottom) Aosta, Rome, and Messina (red dots), as derived from the 2016–2022 ALICENET dataset.

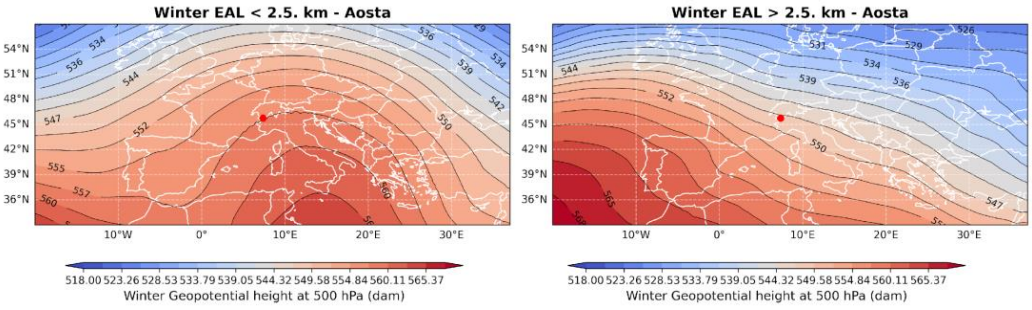


Figure A5. Mean geopotential field at 500 hPa from ERA5 during winter days with elevated aerosol layers below (**left**) and above (**right**) 2.5 km a.s.l. over Aosta (red dot), as derived from the 2016–2022 ALC dataset.

Figure A6 displays the mean difference between the CAMS model and the ALICENET-retrieved PM concentrations within the EALs. The comparison reveals that CAMS underestimates the PM concentrations during EAL events. However, on average, the underestimations remain below 30 μg m^{-3}.

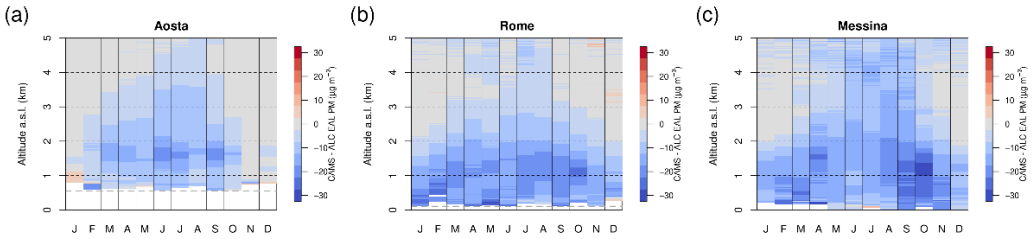


Figure A6. Difference between the CAMS PM_{10} and ALICENET PM estimates within the EALs in (**a**) Aosta, (**b**) Rome, and (**c**) Messina (2018–2022).

Figure A7 shows the seasonal median vertical profiles of different PM_{10} species (dust, wildfires, others) from the CAMS reanalysis for each site. The shaded areas represent the interquartile ranges of the concentrations.

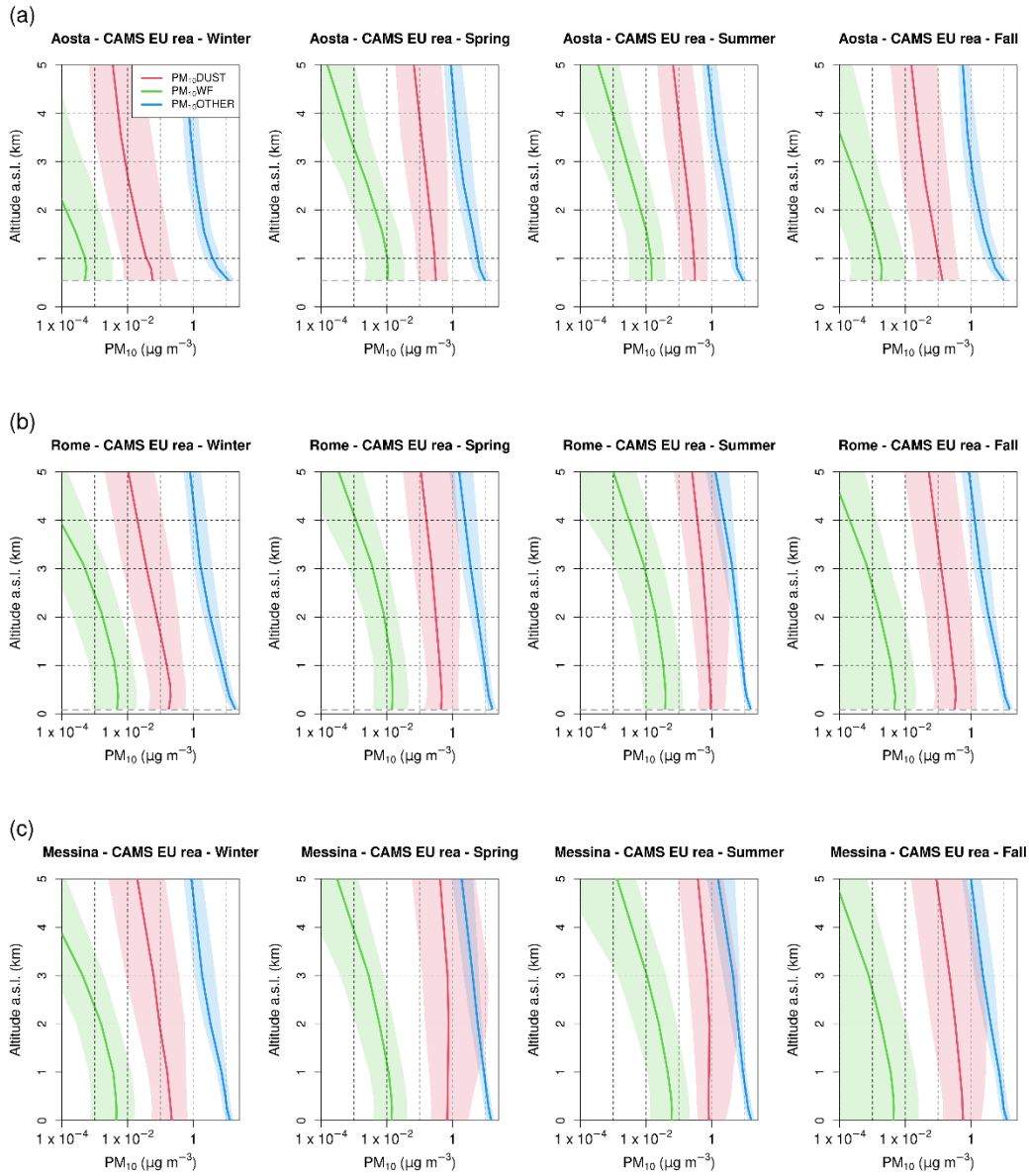


Figure A7. Seasonal median (2018–2022) vertical profiles of the CAMS PM_{10} components: dust (PM_{10}DUST, red), wildfire (PM_{10}WF, green), and other components (PM_{10}OTHER = PM_{10}TOT − PM_{10}DUST − PM_{10}WF, light blue) over (**a**) Aosta, (**b**) Rome, and (**c**) Messina. The shaded areas represent the interquartile ranges. Note the log scale on the x-axis.

References

1. Bellouin, N.; Quaas, J.; Gryspeerdt, E.; Kinne, S.; Stier, P.; Watson-Parris, D.; Boucher, O.; Carslaw, K.S.; Christensen, M.; Daniau, A.; et al. Bounding Global Aerosol Radiative Forcing of Climate Change. *Rev. Geophys.* **2020**, *58*, e2019RG000660. [CrossRef] [PubMed]
2. Wall, C.J.; Storelvmo, T.; Possner, A. Global observations of aerosol indirect effects from marine liquid clouds. *Atmos. Chem. Phys.* **2023**, *23*, 13125–13141. [CrossRef]
3. Stier, P.; van den Heever, S.C.; Christensen, M.W.; Gryspeerdt, E.; Dagan, G.; Saleeby, S.M.; Bollasina, M.; Donner, L.; Emanuel, K.; Ekman, A.M.L.; et al. Multifaceted aerosol effects on precipitation. *Nat. Geosci.* **2024**, *17*, 719–732. [CrossRef]
4. Fuzzi, S.; Baltensperger, U.; Carslaw, K.; Decesari, S.; Van Der Gon, H.D.; Facchini, M.C.; Fowler, D.; Koren, I.; Langford, B.; Lohmann, U.; et al. Particulate matter, air quality and climate: Lessons learned and future needs. *Atmos. Chem. Phys.* **2015**, *15*, 8217–8299. [CrossRef]
5. World Health Statistics 2024: Monitoring Health for the SDGs, Sustainable Development Goals. 2024. Available online: https://www.who.int/publications/i/item/9789240094703 (accessed on 9 December 2024).
6. World Meteorological Organization (WMO). The 2022 GCOS ECVs Requirements (GCOS 245). GCOS. 2022. Available online: https://library.wmo.int/idurl/4/58111 (accessed on 9 December 2024).
7. Raptis, I.-P.; Kazadzis, S.; Amiridis, V.; Gkikas, A.; Gerasopoulos, E.; Mihalopoulos, N. A decade of aerosol optical properties measurements over Athens, Greece. *Atmosphere* **2020**, *11*, 154. [CrossRef]
8. Vogel, A.; Alessa, G.; Scheele, R.; Weber, L.; Dubovik, O.; North, P.; Fiedler, S. Uncertainty in aerosol optical depth from modern aerosol-climate models, reanalyses, and satellite products. *J. Geophys. Res.* **2022**, *127*, e2021JD035483. [CrossRef]
9. Tuna Tuygun, G.; Elbir, T. Comparative analysis of CAMS aerosol optical depth data and AERONET observations in the Eastern Mediterranean over 19 years. *Environ. Sci. Pollut. Res. Int.* **2024**, *31*, 27069–27084. [CrossRef]
10. Peters, A. Ambient air pollution and Alzheimer's disease: The role of the composition of fine particles. *Proc. Natl. Acad. Sci. USA* **2023**, *120*, e2220028120. [CrossRef]
11. Directive—EU—2024/2881—EN—EUR-Lex. Available online: http://data.europa.eu/eli/dir/2024/2881/oj (accessed on 9 December 2024).
12. Fountoulakis, I.; Papachristopoulou, K.; Proestakis, E.; Amiridis, V.; Kontoes, C.; Kazadzis, S. Effect of aerosol vertical distribution on the modeling of solar radiation. *Remote Sens.* **2022**, *14*, 1143. [CrossRef]
13. Napoli, A.; Desbiolles, F.; Parodi, A.; Pasquero, C. Aerosol indirect effects in complex-orography areas: A numerical study over the Great Alpine Region. *Atmos. Chem. Phys.* **2022**, *22*, 3901–3909. [CrossRef]
14. Boucher, O.; Randall, D.; Artaxo, P.; Bretherton, C.; Feingold, G.; Forster, P.; Kerminen, V.M.; Kondo, Y.; Liao, H.; Lohmann, U.; et al. Clouds Aerosols. In *Clouds Aerosols: Climate Change 2013: Physical Science Basis. Contribution Working Group I Fifth Assessment Report Intergovernmental Panel Climate Change*; Cambridge University Press: Cambridge, UK; New York, NY, USA, 2013.
15. Balestrini, R.; Diémoz, H.; Freppaz, M.; Delconte, C.; Caschetto, M.; Matiatos, I. Nitrogen atmospheric deposition in a high-altitude Alpine environment: A chemical and isotopic approach to investigate the influence from anthropized areas. *Atmos. Environ.* **2024**, *328*, 120513. [CrossRef]
16. Di Mauro, B.; Garzonio, R.; Rossini, M.; Filippa, G.; Pogliotti, P.; Galvagno, M.; di Cella, U.M.; Migliavacca, M.; Baccolo, G.; Clemenza, M.; et al. Saharan dust events in the European Alps: Role in snowmelt and geochemical characterization. *Cryosphere* **2019**, *13*, 1147–1165. [CrossRef]
17. Fasano, G.; Diémoz, H.; Fountoulakis, I.; Cassardo, C.; Kudo, R.; Siani, A.M.; Ferrero, L. Vertical profile of the clear-sky aerosol direct radiative effect in an Alpine valley, by the synergy of ground-based measurements and radiative transfer simulations. *Bull. Atmos. Sci. Technol.* **2021**, *2*, 11. [CrossRef]
18. Barreto, Á.; Cuevas, E.; García, R.D.; Carrillo, J.; Prospero, J.M.; Ilić, L.; Basart, S.; Berjón, A.J.; Marrero, C.L.; Hernández, Y.; et al. Long-term characterisation of the vertical structure of the Saharan Air Layer over the Canary Islands using lidar and radiosonde profiles: Implications for radiative and cloud processes over the subtropical Atlantic Ocean. *Atmos. Chem. Phys.* **2022**, *22*, 739–763. [CrossRef]
19. Gobbi, G.; Barnaba, F.; Di Liberto, L.; Bolignano, A.; Lucarelli, F.; Nava, S.; Perrino, C.; Pietrodangelo, A.; Basart, S.; Costabile, F.; et al. An inclusive view of Saharan dust advections to Italy and the Central Mediterranean. *Atmos. Environ.* **2019**, *201*, 242–256. [CrossRef]
20. Diémoz, H.; Barnaba, F.; Magri, T.; Pession, G.; Dionisi, D.; Pittavino, S.; Tombolato, I.K.F.; Campanelli, M.; Della Ceca, L.S.; Hervo, M.; et al. Transport of Po Valley aerosol pollution to the northwestern Alps—Part 1: Phenomenology. *Atmos. Chem. Phys.* **2019**, *19*, 3065–3095. [CrossRef]
21. Diémoz, H.; Gobbi, G.P.; Magri, T.; Pession, G.; Pittavino, S.; Tombolato, I.K.F.; Campanelli, M.; Barnaba, F. Transport of Po Valley aerosol pollution to the northwestern Alps—Part 2: Long-term impact on air quality. *Atmos. Chem. Phys.* **2019**, *19*, 10129–10160. [CrossRef]

22. Kotthaus, S.; Bravo-Aranda, J.A.; Coen, M.C.; Guerrero-Rascado, J.L.; Costa, M.J.; Cimini, D.; O'Connor, E.J.; Hervo, M.; Alados-Arboledas, L.; Jiménez-Portaz, M.; et al. Atmospheric boundary layer height from ground-based remote sensing: A review of capabilities and limitations. *Atmos. Meas. Tech.* **2023**, *16*, 433–479. [CrossRef]
23. Lampilahti, J.; Leino, K.; Manninen, A.; Poutanen, P.; Franck, A.; Peltola, M.; Hietala, P.; Beck, L.; Dada, L.; Quéléver, L.; et al. Aerosol particle formation in the upper residual layer. *Atmos. Chem. Phys.* **2021**, *21*, 7901–7915. [CrossRef]
24. Curci, G.; Ferrero, L.; Tuccella, P.; Barnaba, F.; Angelini, F.; Bolzacchini, E.; Carbone, C.; van der Gon, H.A.C.D.; Facchini, M.C.; Gobbi, G.P.; et al. How much is particulate matter near the ground influenced by upper-level processes within and above the PBL? A summertime case study in Milan (Italy) evidences the distinctive role of nitrate. *Atmos. Chem. Phys.* **2015**, *15*, 2629–2649. [CrossRef]
25. Diémoz, H.; Magri, T.; Pession, G.; Tarricone, C.; Tombolato, I.K.F.; Fasano, G.; Zublena, M. Air quality in the Italian northwestern Alps during year 2020: Assessment of the COVID-19 «lockdown effect» from multi-technique observations and models. *Atmosphere* **2021**, *12*, 1006. [CrossRef]
26. Li, X.; Ma, Y.; Wang, Y.; Wei, W.; Zhang, Y.; Liu, N.; Hong, Y. Vertical distribution of particulate matter and its relationship with planetary boundary layer structure in Shenyang, northeast China. *Aerosol Air Qual. Res.* **2019**, *19*, 2464–2476. [CrossRef]
27. Sun, J.; Veefkind, P.; Nanda, S.; van Velthoven, P.; Levelt, P. The role of aerosol layer height in quantifying aerosol absorption from ultraviolet satellite observations. *Atmos. Meas. Tech.* **2019**, *12*, 6319–6340. [CrossRef]
28. Li, C.; Li, J.; Dubovik, O.; Zeng, Z.-C.; Yung, Y.L. Impact of aerosol vertical distribution on Aerosol Optical Depth retrieval from passive satellite sensors. *Remote Sens.* **2020**, *12*, 1524. [CrossRef]
29. Rogozovsky, I.; Ansmann, A.; Althausen, D.; Heese, B.; Engelmann, R.; Hofer, J.; Baars, H.; Schechner, Y.; Lyapustin, A.; Chudnovsky, A. Impact of aerosol layering, complex aerosol mixing, and cloud coverage on high-resolution MAIAC aerosol optical depth measurements: Fusion of lidar, AERONET, satellite, and ground-based measurements. *Atmos Environ.* **2021**, *247*, 118163. [CrossRef]
30. De Leeuw, G.; van der A, R.; Bai, J.; Hoed, M.D.; Ding, J.; Guo, J.; Li, Z.; Zhang, Y.; Fan, C.; Qin, K.; et al. Remote sensing of air pollutants in China to study the effects of emission reduction policies on air quality. *J. Atmos. Sol. Terr. Phys.* **2024**, *265*, 106392. [CrossRef]
31. Koffi, B.; Schulz, M.; Bréon, F.; Dentener, F.; Steensen, B.M.; Griesfeller, J.; Winker, D.; Balkanski, Y.; Bauer, S.E.; Bellouin, N.; et al. Evaluation of the aerosol vertical distribution in global aerosol models through comparison against CALIOP measurements: AeroCom phase II results. *J. Geophys. Res.* **2016**, *121*, 7254–7283. [CrossRef]
32. Pappalardo, G.; Amodeo, A.; Apituley, A.; Comeron, A.; Freudenthaler, V.; Linné, H.; Ansmann, A.; Bösenberg, J.; D'Amico, G.; Mattis, I.; et al. EARLINET: Towards an advanced sustainable European aerosol lidar network. *Atmos. Meas. Tech.* **2014**, *7*, 2389–2409. [CrossRef]
33. Levin, I.; Karstens, U.; Eritt, M.; Maier, F.; Arnold, S.; Rzesanke, D.; Hammer, S.; Ramonet, M.; Vítková, G.; Conil, S.; et al. A dedicated flask sampling strategy developed for Integrated Carbon Observation System (ICOS) stations based on CO_2 and CO measurements and Stochastic Time-Inverted Lagrangian Transport (STILT) footprint modelling. *Atmos. Chem. Phys.* **2020**, *20*, 11161–11180. [CrossRef]
34. Wiegner, M.; Madonna, F.; Binietoglou, I.; Forkel, R.; Gasteiger, J.; Geiß, A.; Pappalardo, G.; Schäfer, K.; Thomas, W. What is the benefit of ceilometers for aerosol remote sensing? An answer from EARLINET. *Atmos. Meas. Tech.* **2014**, *7*, 1979–1997. [CrossRef]
35. Osborne, M.J.; de Leeuw, J.; Witham, C.; Schmidt, A.; Beckett, F.; Kristiansen, N.; Buxmann, J.; Saint, C.; Welton, E.J.; Fochesatto, J.; et al. The 2019 Raikoke volcanic eruption—Part 2: Particle-phase dispersion and concurrent wildfire smoke emissions. *Atmos. Chem. Phys.* **2022**, *22*, 2975–2997. [CrossRef]
36. Rizza, U.; Avolio, E.; Morichetti, M.; Di Liberto, L.; Bellini, A.; Barnaba, F.; Virgili, S.; Passerini, G.; Mancinelli, E. On the interplay between desert dust and meteorology based on WRF-Chem simulations and remote sensing observations in the Mediterranean basin. *Remote Sens.* **2023**, *15*, 435. [CrossRef]
37. Flentje, H.; Mattis, I.; Kipling, Z.; Rémy, S.; Thomas, W. Evaluation of ECMWF IFS-AER (CAMS) operational forecasts during cycle 41r1–46r1 with calibrated ceilometer profiles over Germany. *Geosci. Model. Dev.* **2021**, *14*, 1721–1751. [CrossRef]
38. Illingworth, A.J.; Cimini, D.; Haefele, A.; Haeffelin, M.; Hervo, M.; Kotthaus, S.; Löhnert, U.; Martinet, P.; Mattis, I.; O'connor, E.J.; et al. How can existing ground-based profiling instruments improve European weather forecasts? *Bull. Am. Meteorol. Soc.* **2019**, *100*, 605–619. [CrossRef]
39. Personnel Directory. Pubs.GISS: Teixeira et al.: Toward a Global Planetary Boundary Layer Observing System: The NASA PBL Incubation. 2021. Available online: https://pubs.giss.nasa.gov/abs/te07200b.html (accessed on 9 December 2024).
40. Caicedo, V.; Delgado, R.; Sakai, R.; Knepp, T.; Williams, D.; Cavender, K.; Lefer, B.; Szykman, J. An automated common algorithm for planetary boundary layer retrievals using aerosol lidars in support of the U.S. EPA Photochemical Assessment Monitoring Stations Program. *J. Atmos. Ocean. Technol.* **2020**, *37*, 1847–1864. [CrossRef]

41. Barnaba, F.; Alvan Romero, N.; Bolignano, A.; Basart, S.; Renzi, M.; Stafoggia, M. Multiannual assessment of the desert dust impact on air quality in Italy combining PM10 data with physics-based and geostatistical models. *Environ. Int.* **2022**, *163*, 107204. [CrossRef]
42. Scollo, S.; Prestifilippo, M.; Bonadonna, C.; Cioni, R.; Corradini, S.; Degruyter, W.; Rossi, E.; Silvestri, M.; Biale, E.; Carparelli, G.; et al. Near-real-time tephra fallout assessment at mt. Etna, Italy. *Remote Sens.* **2019**, *11*, 2987. [CrossRef]
43. Bellini, A.; Diémoz, H.; Di Liberto, L.; Gobbi, G.P.; Bracci, A.; Pasqualini, F.; Barnaba, F. ALICENET—An Italian network of automated lidar ceilometers for four-dimensional aerosol monitoring: Infrastructure, data processing, and applications. *Atmos. Meas. Tech.* **2024**, *17*, 6119–6144. [CrossRef]
44. Dionisi, D.; Barnaba, F.; Diémoz, H.; Di Liberto, L.; Gobbi, G.P. A multiwavelength numerical model in support of quantitative retrievals of aerosol properties from automated lidar ceilometers and test applications for AOT and PM10 estimation. *Atmos. Meas. Tech.* **2018**, *11*, 6013–6042. [CrossRef]
45. Douros, J.; Eskes, H.; van Geffen, J.; Boersma, K.F.; Compernolle, S.; Pinardi, G.; Blechschmidt, A.-M.; Peuch, V.-H.; Colette, A.; Veefkind, P. Comparing Sentinel-5P TROPOMI NO2 column observations with the CAMS regional air quality ensemble. *Geosci. Model. Dev.* **2023**, *16*, 509–534. [CrossRef]
46. Lavers, D.A.; Simmons, A.; Vamborg, F.; Rodwell, M.J. An evaluation of ERA5 precipitation for climate monitoring. *Q. J. R. Meteorol. Soc.* **2022**, *148*, 3152–3165. [CrossRef]
47. Struckmeier, C.; Drewnick, F.; Fachinger, F.; Gobbi, G.P.; Borrmann, S. Atmospheric aerosols in Rome, Italy: Sources, dynamics and spatial variations during two seasons. *Atmos. Chem. Phys.* **2016**, *16*, 15277–15299. [CrossRef]
48. Di Bernardino, A.; Iannarelli, A.M.; Casadio, S.; Mevi, G.; Campanelli, M.; Casasanta, G.; Cede, A.; Tiefengraber, M.; Siani, A.M.; Spinei, E.; et al. On the effect of sea breeze regime on aerosols and gases properties in the urban area of Rome, Italy. *Urban. Clim.* **2021**, *37*, 100842. [CrossRef]
49. Giles, D.M.; Sinyuk, A.; Sorokin, M.G.; Schafer, J.S.; Smirnov, A.; Slutsker, I.; Eck, T.F.; Holben, B.N.; Lewis, J.R.; Campbell, J.R.; et al. Advancements in the Aerosol Robotic Network (AERONET) Version 3 database—Automated near-real-time quality control algorithm with improved cloud screening for Sun photometer aerosol optical depth (AOD) measurements. *Atmos. Meas. Tech.* **2019**, *12*, 169–209. [CrossRef]
50. Kudo, R.; Diémoz, H.; Estellés, V.; Campanelli, M.; Momoi, M.; Marenco, F.; Ryder, C.L.; Ijima, O.; Uchiyama, A.; Nakashima, K.; et al. Optimal use of the Prede POM sky radiometer for aerosol, water vapor, and ozone retrievals. *Atmos. Meas. Tech.* **2021**, *14*, 3395–3426. [CrossRef]
51. Hervo, M.; Poltera, Y.; Haefele, A. An empirical method to correct for temperature-dependent variations in the overlap function of CHM15k ceilometers. *Atmos. Meas. Tech.* **2016**, *9*, 2947–2959. [CrossRef]
52. Klett, J.D. Lidar inversion with variable backscatter/extinction ratios. *Appl. Opt.* **1985**, *24*, 1638–1643. [CrossRef]
53. Adam, M.; Putaud, J.P.; Martins dos Santos, S.; Dell'Acqua, A.; Gruening, C. Aerosol hygroscopicity at a regional background site (Ispra) in Northern Italy. *Atmos. Chem. Phys.* **2012**, *12*, 5703–5717. [CrossRef]
54. Giorgino, T. Computing and visualizing dynamic time warping alignments inR: ThedtwPackage. *J. Stat. Softw.* **2009**, *31*, 1–24. [CrossRef]
55. Du, P.; Kibbe, W.A.; Lin, S.M. Improved peak detection in mass spectrum by incorporating continuous wavelet transform-based pattern matching. *Bioinformatics* **2006**, *22*, 2059–2065. [CrossRef]
56. D'Angelo, L.; Rovelli, G.; Casati, M.; Sangiorgi, G.; Perrone, M.G.; Bolzacchini, E.; Ferrero, L. Seasonal behavior of PM2.5 deliquescence, crystallization, and hygroscopic growth in the Po Valley (Milan): Implications for remote sensing applications. *Atmos. Res.* **2016**, *176–177*, 87–95. [CrossRef]
57. Hersbach, H.; Bell, B.; Berrisford, P.; Hirahara, S.; Horányi, A.; Muñoz-Sabater, J.; Nicolas, J.; Peubey, C.; Radu, R.; Schepers, D.; et al. The ERA5 global reanalysis. *Q. J. R. Meteorol. Soc.* **2020**, *146*, 1999–2049. [CrossRef]
58. C3S Data. Available online: https://cds.climate.copernicus.eu/ (accessed on 11 December 2024).
59. CAMS Data. Available online: https://atmosphere.copernicus.eu/european-air-quality-reanalysis (accessed on 13 January 2025).
60. Galmarini, S.; Kioutsioukis, I.; Solazzo, E.; Alyuz, U.; Balzarini, A.; Bellasio, R.; Christensen, J.H. Two-scale multi-model ensemble: Is a hybrid ensemble of opportunity telling us more? *Atmos. Chem. Phys.* **2018**, *18*, 8727–8744. [CrossRef] [PubMed]
61. Menut, L.; Mailler, S.; Siour, G.; Bessagnet, B.; Turquety, S.; Rea, G.; Briant, R.; Mallet, M.; Sciare, J.; Formenti, P. Analysis of the atmospheric composition during the summer 2013 over the Mediterranean area using the CHARMEX measurements and the CHIMERE model. *Atmos. Chem. Phys. Discuss.* **2014**, *16*, 23075–23123. [CrossRef]
62. Simpson, D.; Benedictow, A.; Berge, H.; Bergström, R.; Emberson, L.D.; Fagerli, H.; Flechard, C.R.; Hayman, G.D.; Gauss, M.; Jonson, J.E.; et al. The EMEP MSC-W chemical transport model—Technical description. *Atmos. Chem. Phys.* **2012**, *12*, 7825–7865. [CrossRef]
63. Memmesheimer, M.; Jakobs, H.J.; Friese, E.; Müller, W.J.; Ebel, A.; Feldmann, H. Episodes of high concentrations of PM10 and PM2.5 over Europe in winter 2002/2003: Meteorological conditions and chemical composition as calculated with a complex operational short-term air-quality model. *J. Aerosol. Sci.* **2004**, *35*, 1251–1262. [CrossRef]

64. Manders, A.M.M.; Builtjes, P.J.H.; Curier, L.; van der Gon, H.A.C.D.; Hendriks, C.; Jonkers, S.; Kranenburg, R.; Kuenen, J.J.P.; Segers, A.J.; Timmermans, R.M.A.; et al. Curriculum vitae of the LOTOS–EUROS (v2.0) chemistry transport model. *Geosci. Model. Dev.* **2017**, *10*, 4145–4173. [CrossRef]
65. Robertson, L.; Langner, J.; Engardt, M. An eulerian limited-area atmospheric transport model. *J. Appl. Meteorol.* **1999**, *38*, 190–210. [CrossRef]
66. Guth, J.; Josse, B.; Marécal, V.; Joly, M.; Hamer, P. First implementation of secondary inorganic aerosols in the MOCAGE version R2.15.0 chemistry transport model. *Geosci. Model. Dev.* **2016**, *9*, 137–160. [CrossRef]
67. Sofiev, M.; Vira, J.; Kouznetsov, R.; Prank, M.; Soares, J.; Genikhovich, E. Construction of an Eulerian atmospheric dispersion model based on the advection algorithm of M. Galperin: Dynamic cores v.4 and 5 of SILAM v.5.5. *Geosci. Model. Dev. Discuss.* **2015**, *8*, 2905–2947. [CrossRef]
68. Christensen, J.H. The Danish eulerian hemispheric model—A three-dimensional air pollution model used for the arctic. *Atmos. Environ.* **1997**, *31*, 4169–4191. [CrossRef]
69. Kaminski, J.W.; Neary, L.; Struzewska, J.; McConnell, J.C.; Lupu, A.; Jarosz, J.; Toyota, K.; Gong, S.L.; Côté, J.; Liu, X.; et al. GEM-AQ, an on-line global multiscale chemical weather modelling system: Model description and evaluation of gas phase chemistry processes. *Atmos. Chem. Phys.* **2008**, *8*, 3255–3281. [CrossRef]
70. Bonanno, R.; Lacavalla, M.; Sperati, S. A new high-resolution Meteorological Reanalysis Italian Dataset: MERIDA. *Q. J. R. Meteorol. Soc.* **2019**, *145*, 1756–1779. [CrossRef]
71. MERIDA. Available online: https://merida.rse-web.it/ (accessed on 11 December 2024).
72. Gkikas, A.; Basart, S.; Hatzianastassiou, N.; Marinou, E.; Amiridis, V.; Kazadzis, S.; Pey, J.; Querol, X.; Jorba, O.; Gassó, S.; et al. Mediterranean intense desert dust outbreaks and their vertical structure based on remote sensing data. *Atmos. Chem. Phys.* **2016**, *16*, 8609–8642. [CrossRef]
73. Angevine, W.M.; Hare, J.E.; Fairall, C.W.; Wolfe, D.E.; Hill, R.J.; Brewer, W.A.; White, A.B. Structure and formation of the highly stable marine boundary layer over the Gulf of Maine. *J. Geophys. Res.* **2006**, *111*, D23. [CrossRef]
74. Bellini, A.; Golzio, A.; Magri, T.; Ferrarese, S.; Pession, G.; Manfrin, M. Sensitivity of pollutant concentrations to the turbulence schemes of a dispersion modelling chain over complex orography. *Atmosphere* **2022**, *13*, 167. [CrossRef]
75. Riccobono, F.; Schobesberger, S.; Scott, C.E.; Dommen, J.; Ortega, I.K.; Rondo, L.; Almeida, J.; Amorim, A.; Bianchi, F.; Breitenlechner, M.; et al. Oxidation products of biogenic emissions contribute to nucleation of atmospheric particles. *Science* **2014**, *344*, 717–721. [CrossRef]
76. Barnaba, F.; Putaud, J.P.; Gruening, C.; dell'Acqua, A.; Dos Santos, S. Annual cycle in co-located in situ, total-column, and height-resolved aerosol observations in the Po Valley (Italy): Implications for ground-level particulate matter mass concentration estimation from remote sensing. *J. Geophys. Res.* **2010**, *115*, D19209. [CrossRef]
77. Fernandes, A.; Pietruczuk, A.; Szkop, A.; Krzyścin, J. Aerosol layering in the free troposphere over the Industrial City of raciborz in southwest Poland and its influence on surface UV radiation. *Atmosphere* **2021**, *12*, 812. [CrossRef]
78. Barreto, A.; Román, R.; Cuevas, E.; Pérez-Ramírez, D.; Berjón, A.J.; Kouremeti, N.; Kazadzis, S.; Gröbner, J.; Mazzola, M.; Toledano, C.; et al. Evaluation of night-time aerosols measurements and lunar irradiance models in the frame of the first multi-instrument nocturnal intercomparison campaign. *Atmos. Environ.* **2019**, *202*, 190–211. [CrossRef]
79. Serafin, S.; Adler, B.; Cuxart, J.; De Wekker, S.F.J.; Gohm, A.; Grisogono, B.; Kalthoff, N.; Kirshbaum, D.J.; Rotach, M.W.; Schmidli, J.; et al. Exchange processes in the atmospheric boundary layer over mountainous terrain. *Atmosphere* **2018**, *9*, 102. [CrossRef]
80. Kotthaus, S.; Haeffelin, M.; Drouin, M.-A.; Dupont, J.-C.; Grimmond, S.; Haefele, A.; Hervo, M.; Poltera, Y.; Wiegner, M. Tailored algorithms for the detection of the atmospheric boundary layer height from common automatic lidars and ceilometers (ALC). *Remote Sens.* **2020**, *12*, 3259. [CrossRef]
81. De Tomasi, F.; Perrone, M.R. PBL and dust layer seasonal evolution by lidar and radiosounding measurements over a peninsular site. *Atmos. Res.* **2006**, *80*, 86–103. [CrossRef]
82. Coen, M.C.; Andrews, E.; Aliaga, D.; Andrade, M.; Angelov, H.; Bukowiecki, N.; Ealo, M.; Fialho, P.; Flentje, H.; Hallar, A.G.; et al. Identification of topographic features influencing aerosol observations at high altitude stations. *Atmos. Chem. Phys.* **2018**, *18*, 12289–12313. [CrossRef]
83. Shang, X.; Lipponen, A.; Filioglou, M.; Sundström, A.-M.; Parrington, M.; Buchard, V.; Darmenov, A.S.; Welton, E.J.; Marinou, E.; Amiridis, V.; et al. Monitoring biomass burning aerosol transport using CALIOP observations and reanalysis models: A Canadian wildfire event in 2019. *Atmos. Chem. Phys.* **2024**, *24*, 1329–1344. [CrossRef]
84. Merdji, A.B.; Lu, C.; Xu, X.; Mhawish, A. Long-term three-dimensional distribution and transport of Saharan dust: Observation from CALIPSO, MODIS, and reanalysis data. *Atmos. Res.* **2023**, *286*, 106658. [CrossRef]
85. Israelevich, P.; Ganor, E.; Alpert, P.; Kishcha, P.; Stupp, A. Predominant transport paths of Saharan dust over the Mediterranean Sea to Europe. *J. Geophys. Res.* **2012**, *117*, D2. [CrossRef]
86. Tositti, L.; Brattich, E.; Cassardo, C.; Morozzi, P.; Bracci, A.; Marinoni, A.; Di Sabatino, S.; Porcù, F.; Zappi, A. Development and evolution of an anomalous Asian dust event across Europe in March 2020. *Atmos. Chem. Phys.* **2022**, *22*, 4047–4073. [CrossRef]

87. Sicard, M.; Barragan, R.; Dulac, F.; Alados-Arboledas, L.; Mallet, M. Aerosol optical, microphysical and radiative properties at regional background insular sites in the western Mediterranean. *Atmos. Chem. Phys.* **2016**, *16*, 12177–12203. [CrossRef]
88. Barnaba, F.; Angelini, F.; Curci, G.; Gobbi, G.P. An important fingerprint of wildfires on the European aerosol load. *Atmos. Chem. Phys.* **2011**, *11*, 10487–10501. [CrossRef]
89. Barnaba, F.; Gobbi, G.P. Aerosol seasonal variability over the Mediterranean region and relative impact of maritime, continental and Saharan dust particles over the basin from MODIS data in the year 2001. *Atmos. Chem. Phys.* **2004**, *4*, 2367–2391. [CrossRef]
90. Scollo, S.; Boselli, A.; Coltelli, M.; Leto, G.; Pisani, G.; Prestifilippo, M.; Spinelli, N.; Wang, X. Volcanic ash concentration during the 12 August 2011 Etna eruption. *Geophys. Res. Lett.* **2015**, *42*, 2634–2641. [CrossRef]
91. Cuevas, E.; Gómez-Peláez, A.; Rodríguez, S.; Terradellas, E.; Basart, S.; García, R.; García, O.; Alonso-Pérez, S. The pulsating nature of large-scale Saharan dust transport as a result of interplays between mid-latitude Rossby waves and the North African Dipole Intensity. *Atmos. Environ.* **2017**, *167*, 586–602. [CrossRef]
92. Pey, J.; Perez, N.; Querol, X.; Alastuey, A.; Forastiere, F.; Stafoggia, M.; Study Group. MED-PARTICLES. Saharan dust and forest fires in Southern Europe in the period 2001–2011: Estimation and geographical distribution. *Environ. Health Perspect.* **2013**, *2013*, 4546. [CrossRef]
93. Gkikas, A.; Hatzianastassiou, N.; Mihalopoulos, N.; Katsoulis, V.; Kazadzis, S.; Pey, J.; Querol, X.; Torres, O. The regime of desert dust episodes in the Mediterranean based on contemporary satellite observations and ground measurements. *Atmos. Chem. Phys. Discuss.* **2013**, *13*, 16247–16299. [CrossRef]
94. Dayan, U.; Ricaud, P.; Zbinden, R.; Dulac, F. Atmospheric pollution over the eastern Mediterranean during summer—A review. *Atmos. Chem. Phys.* **2017**, *17*, 13233–13263. [CrossRef]
95. Putaud, J.P.; Cavalli, F.; Martins dos Santos, S.; Dell'Acqua, A. Long-term trends in aerosol optical characteristics in the Po Valley, Italy. *Atmos. Chem. Phys.* **2014**, *14*, 9129–9136. [CrossRef]
96. Pandolfi, M.; Tobias, A.; Alastuey, A.; Sunyer, J.; Schwartz, J.; Lorente, J.; Pey, J.; Querol, X. Effect of atmospheric mixing layer depth variations on urban air quality and daily mortality during Saharan dust outbreaks. *Sci. Total. Environ.* **2014**, *494–495*, 283–289. [CrossRef]

Disclaimer/Publisher's Note: The statements, opinions and data contained in all publications are solely those of the individual author(s) and contributor(s) and not of MDPI and/or the editor(s). MDPI and/or the editor(s) disclaim responsibility for any injury to people or property resulting from any ideas, methods, instructions or products referred to in the content.